https://doi.org/10.5194/egusphere-2025-291
Preprint. Discussion started: 11 February 2025

Influences on Chemical Distribution Patterns across the west Greenland Shelf: The Roles of Ocean Currents, Sea Ice Melt, and Freshwater Runoff

Claudia E. Schmidt[1,2], Tristan Zimmermann[3], Katarzyna Koziorowska[4], Daniel Pröfrock[3], Helmuth Thomas[1,2]

[1]Helmholtz-Zentrum Hereon, Institute of Carbon Cycles, 21502, Geesthacht, Germany
[2]Carl von Ossietzky University Oldenburg, Institute for Chemistry and Biology of the Marine Environment, 26129, Oldenburg, Germany
[3]Helmholtz-Zentrum Hereon, Institute of Coastal Environmental Chemistry, 21502, Geesthacht, Germany
[4]Institute of Oceanology Polish Academy of Sciences, Department of Marine Chemistry and Biochemistry, 81-712, Sopot, Poland

Correspondence to: Helmuth Thomas (helmuth.thomas@hereon.de)

Abstract The west Greenland shelf is a dynamic marine environment influenced by various physicochemical and biological processes. This study provides an overview of the main factors affecting the distribution of macronutrients, carbonate system parameters, and dissolved trace elements during late summer. Key drivers include major ocean currents, melting sea ice, and terrestrial freshwater runoff, each uniquely contributing to the cycling and spatial distribution of chemical constituents. Major ocean currents, such as the southward-moving Baffin Island Current (BIC) and the northward-moving West Greenland Current (WGC), shape the chemical composition of shelf waters by introducing water masses with distinct chemical signatures. Melting sea ice is an important source of freshwater and dissolved constituents for the marine environment. The east-to-west direction of sea ice retreat creates nutrient gradients, with low nutrient levels in highly productive shelf waters and high nutrient levels in areas with prolonged ice cover. This process also affects the carbonate system, leading to changes in pH and aragonite saturation states, which is critical for the health of marine organisms. Terrestrial freshwater runoff, particularly from the Greenland Ice Sheet (GIS), replenishes macronutrients in the photic zone, stimulating primary production and creating important CO_2 sinks. However, surface waters become more susceptible to acidification by the input of poorly buffered glacial freshwater. Understanding these key drivers is essential for forecasting future changes in the marine chemistry and biology of the west Greenland shelf, especially in the context of ongoing climate change within this high-latitude region.

https://doi.org/10.5194/egusphere-2025-291
Preprint. Discussion started: 11 February 2025

1 Introduction

The physical system of the Arctic Ocean is inevitably changing, with profound implications for primary productivity (PP) and the biogeochemical cycling of nutrients and carbon on shelves and in deep basins (Juranek, 2022). The complex coastal current system that connects the continental shelves of Greenland with the Arctic Ocean, the North Atlantic Ocean, and the Pacific Ocean strongly impacts PP (Vernet et al., 2021), creating an important environment for biota and fisheries (Krawczyk et al., 2021). The major ocean currents on the west side of Greenland are shown in Fig. 1 a. The circulation across the west Greenland shelf and Baffin Bay is dominated by the opposing direction of the Baffin Island Current (BIC) and West Greenland Current (WGC) (Curry et al., 2011). On the western side of Baffin Bay, the surface-intensified BIC transports water from the Alaskan shelf and the western Beaufort Sea through the narrow and shallow channels of the Canadian Arctic Archipelago (CAA) across Davis Strait into the Labrador Sea (Nares Strait, Jones Sound, and Lancaster Sound) (Aksenov et al., 2016; Curry et al., 2011; Tang et al., 2004). Arctic waters of Pacific origin that enter Baffin Bay through the CAA have been described to be a source of dissolved trace elements (e.g., dMn, dFe, dCu, dNi) (Colombo et al., 2020; Colombo et al., 2021; Jensen et al., 2022) and carbon (Azetsu-Scott et al., 2010; Burgers et al., 2024; Shadwick et al., 2011b). Further south, Davis Strait has been suggested as a gateway for the transport of dissolved trace elements (Krisch et al., 2022a) and dissolved inorganic nitrogen (Juranek, 2022) from the Arctic to the North Atlantic Ocean. On the eastern side of Baffin Bay, the West Greenland Current (WGC) flows northward across Davis Strait and consists of the warm and low-salinity West Greenland Coastal Current (WGCC) on the shelf and the warm and high-salinity West Greenland Slope Current (WGSC) (Curry et al., 2011). Waters of North Atlantic origin have been associated with anthropogenically elevated dissolved lead (dPb) concentrations (Colombo et al., 2019), but also higher productivity and species richness across the west Greenland shelf waters (Krawczyk et al., 2021).

In the last two decades, sea ice concentrations in Baffin Bay and the Labrador Sea have decreased significantly due to climate change (Krawczyk et al., 2021). Reduced sea ice cover has been correlated with an overall increase in productivity and species richness along the west Greenland shelf (Krawczyk et al., 2021; Møller et al., 2023). In all seasonally ice-covered areas, intense but short-lived phytoplankton blooms develop in low-salinity waters at the edge of melting and retreating sea ice from spring to late summer (Niebauer et al., 1995; Perrette et al., 2011). Phytoplankton growth is triggered by the stabilizing effect of sea ice meltwater-induced stratification in surface waters and the increased solar irradiance as the ice cover shrinks (Strass and Nöthig, 1996; Perrette et al., 2011). The newly exposed waters are still nutrient-rich but quickly become depleted after the onset of the bloom (Niebauer et al., 1995). This is why macronutrient distributions (NOx = nitrate + nitrite; phosphate, PO_4^{3-}; silicate, $Si(OH)_4$) in surface waters of Baffin Bay decrease along a west-to-east gradient as they generally follow the ice coverage (Lafond et al., 2019; Tremblay et al., 2002). Although sea ice meltwater is considered a negligible net source of macronutrients, it can significantly enhance trace element concentrations in the receiving waters (Evans and Nishioka, 2019; Hölemann et al., 1999; Kanna et al., 2014; Tovar-Sánchez et al., 2010). Elevated trace element concentrations in Arctic sea ice have been linked to entrained sediments (Measures, 1999) or atmospheric deposition from continuous emissions in highly industrialized countries (McConnell and Edwards, 2008). The carbonate system of Baffin Bay is influenced by sea ice

https://doi.org/10.5194/egusphere-2025-291
Preprint. Discussion started: 11 February 2025

meltwater, as it has the potential to supply additional alkalinity (AT) (Jones et al., 1983). During sea ice formation, ikaite ($CaCO_3 \cdot 6H_2O$) precipitates within the sea ice and is reintroduced to the water column during ice melt, resulting in higher AT concentrations relative to dissolved inorganic carbon (CT), lower pCO_2 conditions, and higher pH as well as aragonite saturation state (Ω Aragonite) in surface waters (Fransson et al., 2013; Rysgaard et al., 2011; Rysgaard et al., 2012).

The mass loss of the Greenland Ice Sheet (GIS) has increased sixfold since the 1980s, with the region northwards of Davis Strait experiencing the largest mass loss (Mouginot et al., 2019; Wouters and Sasgen, 2022). The export of glacial runoff from the GIS alters shelf and slope waters significantly, thus impacting PP in near-coastal regions (Hawkings et al., 2015; Juul-Pedersen et al., 2015). The glacier-derived freshwater alters marine concentrations of macronutrients (Hawkings et al., 2015; Hawkings et al., 2016; Hawkings et al., 2017; Hendry et al., 2019) and dissolved trace elements (Hawkings et al., 2020; Krause et al., 2021), impacts the hydrography, and facilitates the upwelling of nutrient-rich deep water (Meire et al., 2017; Juul-Pedersen et al., 2015). This fertilizes adjacent marine systems and promotes high levels of biological productivity (Bhatia et al., 2013; Hawkings et al., 2020; Oksman et al., 2022). Glacial freshwater exhibits low AT and carbonate ion concentration (CO_3^{2-}) relative to marine waters, reducing the capacity of glacially modified waters to resist changes in pH from the uptake of atmospheric CO_2 (Bates and Mathis, 2009; Chierici and Fransson, 2009; Fransson et al., 2015). In surface waters of the Greenlandic coast, AT dilution from glacial meltwater has been observed to drive corrosive conditions with an overall decrease in Ω Aragonite and pH (Henson et al., 2023; Shadwick et al., 2013). Photosynthetic CO_2 uptake can mitigate this negative effect of AT dilution, as PP reduces CT and $pCO2$ concentrations in surface waters and increases the carbonate saturation state (Chierici and Fransson, 2009; Hopwood et al., 2020; Meire et al., 2015).

In this study, we present recent (July 2021) measurements of the marine carbonate system, along with nutrient concentrations and dissolved (d; < 0.45 µm) trace element concentrations across the west Greenland shelf in southern Baffin Bay between 64°N and 71°N (Fig. 1 b). Given the above considerations, the objectives of this study are to: (a) understand the physicochemical processes that influence the internal cycling of chemical constituents in the different water masses of shelf waters; and (b) resolve the regional and spatial differences in the distribution patterns on the west Greenland shelf during late summer that are driven by (i) major ocean currents, (ii) melting sea ice, and (iii) terrestrial freshwater runoff.

https://doi.org/10.5194/egusphere-2025-291
Preprint. Discussion started: 11 February 2025

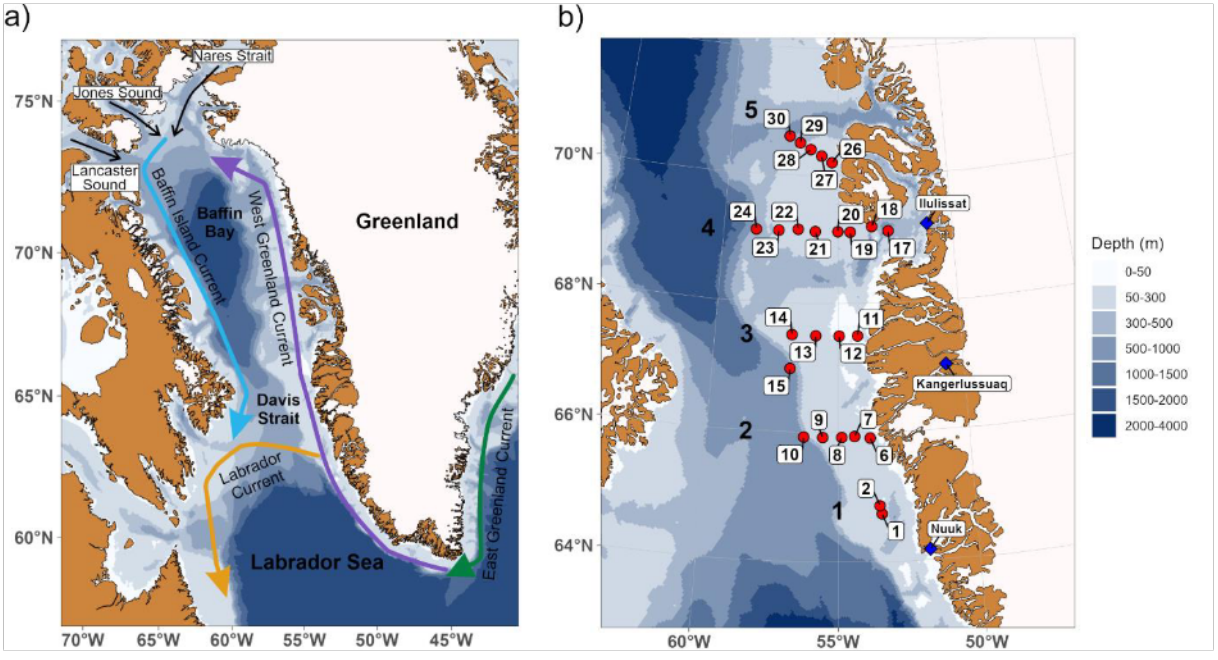

Figure 1: a) Schematic overview of the ocean currents and bathymetry in Baffin Bay and Davis Strait. Colored lines with arrows indicate the direction of different ocean currents. Bathymetry data from the GEBCO 2023 grid (GEBCO Bathymetric Compilation Group 2023, 2023). b) Map of the study area during DANA 6/21 with red points indicating the sampling locations and their affiliation to a certain transect (1-5).

2 Material and Methods

2.1 Study Area

A map of the study area with stations indicated by red dots is given in Fig. 1 b. General information about the selected stations and samples used in this study is provided in Table S 1. Samples were taken along two transects to the south and three transects to the north of Davis Strait along the west Greenland shelf. Transect 1 was located in a shallow area (< 120 m depth) north of Nuuk. Transects 2 and 3 started close to the mouth of Kangerlussuaq Fjord and Nassuttooq Fjord, respectively. Station 15, which is part of transect 3, had to be moved further south because of the presence of sea ice. Transect 4 started in Disko Bay approximately 70 km from the mouth of the Ilulissat Icefjord, where the Jakobshavn Isbræ terminates. Transects 2, 3, and 4 continued westward away from the coast towards the shelf edge. Transect 5 started close to Disko Island and continued towards the northwest.

2.2 Sampling

Water column samples were taken at 25 stations as conductivity-temperature-depth (CTD) casts along five transects during ten consecutive sampling days between 18 and 28 July 2021 on board RV *Dana* (DANA 6/21, Fig. 1 b, Table S 1). A SBE 911 CTD+ unit (Sea-Bird Scientific; Bellevue, USA) was used to collect hydrographic profiles, including temperature, salinity,

https://doi.org/10.5194/egusphere-2025-291
Preprint. Discussion started: 11 February 2025

pressure, and dissolved oxygen. Samples were collected in 10 L Niskin water samplers (Ocean Test Equipment; Fort Lauderdale, USA). Detailed information about each sample is given in Table S 1, with sample IDs corresponding to the respective station and sampling depth.

2.2.1 Macronutrients

Water samples for nutrient analysis were collected in acid-washed 100 mL HDPE (high-density polyethylene) bottles. The bottles were preconditioned three times with sample water before being filled. The samples were stored frozen at -20°C until analysis.

2.2.2 Dissolved trace elements

Bulk samples for multi-element analysis were filled into acid-cleaned 2 L HDPE bottles. The bottles were rinsed three times with sample water before being filled. Immediately after sampling, the water samples were filtered as duplicates using high-purity PFA (Perfluoroalkoxy alkane) filtration bombs (Savillex, Eden Prairie, USA) pressurized with nitrogen 5.0 (Air Liquide Danmark; Taastrup, Denmark) and acid-washed polycarbonate filters (0.45 µm, 47 mm diameter, Whatman, UK) in a clean bench (Erlab; Val de Reuil Cedex, France). More information about the filtration procedure can be found in Przibilla *et al.* (2023). The filtered samples were collected in pre-cleaned 250 mL HDPE bottles and stabilized using trace metal grade HCl (Fisher Scientific; Waltham, USA) before storage and shipping.

2.2.3 Carbonate system parameters

Samples for AT and CT were collected in 300 mL BOD (biological oxygen demand) bottles (Environmental Express, Charleston, USA) with an addition of 300 µL saturated mercury chloride solution (Carl Roth, Karlsruhe, Germany). The bottles were sealed with ground-glass stoppers (Wheaton Science Products, New Jersey, USA), silicone- and halogen-free grease (type M, Apiezon, Manchester, UK), and plastic caps (Wheaton Science Products, New Jersey, USA), leaving no headspace. The samples were stored in darkness at ambient temperature until analysis.

2.3 Sample preparation and chemical analysis

2.3.1 Macronutrients

Nitrite, phosphate, and silicate were measured on a SmartChem 200 discrete analyser (AMS Alliance, Rome, Italy) following the reagent concentrations for the manual method in Hansen and Koroleff (1999), with the inclusion of a 150 g L^{-1} solution of sodium dodecylsulfate as a dispersant for phosphate analysis. Nitrate was measured following the vanadium chloride reduction technique described by Schnetger and Lehners (2014). Community reference material for nutrients in seawater supplied by Kanso Technos Co. LTD, Japan, was used for quality control.

https://doi.org/10.5194/egusphere-2025-291
Preprint. Discussion started: 11 February 2025

2.3.2 Dissolved trace elements

All equipment for trace metal analysis was acid-washed prior to use and rinsed with type I reagent-grade water (resistivity: 18.2 MΩ·cm) obtained from a Milli-Q Integral water purification system (Merck; Darmstadt, Germany) to prevent contamination. Dissolved trace elements (dV, dFe, dMn, dCo, dNi, dCu, dCd, and dPb) in seawater were measured with a seaFAST SP2 system (Elemental Scientific; Omaha, USA) coupled online to an inductively coupled plasma mass spectrometer (ICP-MS) (Agilent 7900, Agilent Technologies; Tokyo, Japan). The seaFAST SP2 system contained two columns filled with Nobias chelate-PA1 resin (HITACHI High-Tech Fielding Corporation; Tokyo, Japan). Detailed operating parameters and instrument configurations are given in Table S 2. More information about the analytical procedure can be found in Ebeling *et al.* (2022). For method validation, the certified reference material (CRM) NASS 7 (National Research Council Canada; Ottawa, Canada) as well as an in-house reference material (KBA-QC) mixed from single element standards (Carl Roth GmbH, Karlsruhe, Germany or Sigma-Aldrich, Missouri, USA) and custom-made multi-element standards (all traceable to NIST standards) of different compositions (Inorganic Ventures, Christiansburg, USA) were used. Recovery rates (between 97 % and 119 %) are given in Table S 3.

2.3.3 Carbonate system parameters

Measurements of AT and CT were performed using a VINDTA 3 C system (Marianda; Kiel, Germany). AT and CT were determined simultaneously by potentiometric titration using an 800 Dosino (Metrohm; Filderstadt, Germany) with an Aquatrode plus (Metrohm; Filderstadt, Germany) and coulometric titration using a CM5017O coulometer (UIC; Illinois, USA), respectively. Both instruments were calibrated against seawater CRMs (Scripps Institution of Oceanography; San Diego, USA) to ensure a precision of ± 1 µmol kg^{-1} for each parameter.

2.4 Data analysis

The raw CTD data were processed and averaged into 0.5 dbar pressure bins. The processed CTD data were used to construct water depth profiles of potential temperature, salinity, potential density, and oxygen (Fig. S 1 to S 5). Calculations were performed using R (version 4.2.2; (R Core Team, 2022)) and RStudio (version 2023.06.0; (Posit team, 2023)). Bivariate, linear data interpolation in combination with a surface approximation using multilevel B-splines with the "interp" function (package akima; (Akima and Gebhardt, 2022)) and the "mba.surf" function (package MBA; (Finley et al., 2022)) was used before plotting.

For trace elements analysis, filtration duplicates were obtained and measured as triplicates ($n = 6$). Outliers were identified using a Dean-Dixon outliers test and removed from further analysis. Mean concentrations (μ) and standard deviation (SD; σ) were estimated, considering twice the SD to represent $\mu \pm 2\sigma$. Limits of detection (LOD) and limits of quantification (LOQ) are given in Table S 3 and were calculated according to DIN 32645:2008-11 by measuring filtrations blanks ($n = 8$), with LOD defined as 3 × SD and LOQ as 10 × SD of the blank (DIN e.V., 2008).

https://doi.org/10.5194/egusphere-2025-291
Preprint. Discussion started: 11 February 2025

The sum parameter NOx for nitrate and nitrite (NOx = nitrate + nitrite) was established and used throughout the discussion. The LOQs for the nutrient analysis are given in Table S 3.

Parameters of the carbonate system (pH, pCO_2, Revelle factor, and Ω Aragonite) were calculated using the CO2Sys Macro (Pierrot et al., 2011) with salinity, temperature, AT and CT as input variables. As input parameters, we used the dissociation constant by Mehrbach et al. (1973), refit by Dickson and Millero (1987), the HSO4- dissociation constant by Dickson (1990) and the seawater pH-scale (Dickson, 1990; Dickson and Millero, 1987; Mehrbach et al., 1973). We used the CO2Sys Macro to calculate temperature-normalized CT (CT_{temp}) according to Wu *et al.* (2019). The calculation was based on the median potential temperature of WGSW (3.23°C) within a depth range of 30 to 50 m, using observed salinity and AT, and the in situ pCO_2 as input parameters.

For statistical analysis, the data of the different parameters were merged according to station and sampling depth, obtaining one data matrix with 17 parameters and 41 observations. Values below LOD were replaced with a random value between zero and LOD. Each parameter was tested for normality (Shapiro-Wilk test, $\alpha = 0.01$) and transformed (log- or Box Cox-transformation) if the normality criteria was not met (Table S 4). The data were standardized, and principal component analysis (PCA) with varimax rotation was performed using the "principal" function (package psych; (Revelle, 2024)). Three principal components (PCs) were selected, considering the Guttman-Kaiser criterion and the trend of the scree plot. A broken stick analysis was performed to distinguish the loading significance of each variable.

3 Results

The distributions of basic oceanographic parameters (salinity, potential temperature, oxygen, Apparent Oxygen Utilization (AOU)), macronutrients (NOx, silicate, phosphate), carbonate system parameters (AT, CT, pH, pCO_2, Revelle factor, Ω Aragonite), and dissolved trace elements (dV, dMn, dFe, dCo, dNi, dCu, dCd, and dPb) are presented in separate sections. The supplementary material (Fig. S 1 to Fig. S 12) provides detailed information on water column profiles and surface water concentration plots for individual parameters. Minimum and maximum values of macronutrients, carbonate system parameters, and trace elements are presented in Table 1.

https://doi.org/10.5194/egusphere-2025-291
Preprint. Discussion started: 11 February 2025

Table 1: Minimum and maximum values of macronutrients, carbonate system parameters and trace elements across the study area.

Parameter	Unit	Minimum		Maximum		Literature data
		Value	Station [Depth in m]	Value	Station [Depth in m]	Min – Max range
NOx	µmol L^{-1}	0.21	13 [30]	17.85	15 [667]	2015: 0.032 – 24.3 [1] 2016: 0.05 – 28.5 [2]
Silicate	µmol L^{-1}	0.51	22 [3]	35.95	15 [667]	2015: 0.32 – 103.7 [1] 2016: 0.11 – 131.4 [2]
Phosphate	µmol L^{-1}	0.12	22 [3]	1.43	15 [667]	2015: 0.46 – 1.97 [1] 2016: 0.06 – 2.2 [2]
AT	µmol kg^{-1}	2062	15 [3]	2305	10 [551]	2015: 2156 – 2294 [4] 2016: 2176 – 2310 [3]
CT	µmol kg^{-1}	1949	15 [3]	2214	15 [667]	2015: 2008 – 2255 [4] 2016: 1937 – 2277 [3]
CT:AT		0.907	17 [3]	0.968	15 [667]	NA
pH		7.86	15 [667]	8.20	15 [32]	2015: 7.40 – 7.81 [1]
pCO_2	µatm	249	15 [32]	559	15 [667]	NA
Revelle factor		11.85	17 [3]	17.80	15 [667]	NA
Ω Aragonite		0.90	15 [667]	2.17	17 [3]	NA
dV	ng L^{-1}	1270 ± 30	24 [3]	1810 ± 60	10 [551]	NA
dMn	ng L^{-1}	54.8 ± 1.8	24 [317]	503 ± 20	12 [37]	13.5 ± 1.7 – 306.0 ± 2.6 [1]
dFe	ng L^{-1}	56.9 ± 2.5	27 [15]	630 ± 30	18 [256]	20.0 ± 0.6 – 112 ± 8 [1]
dCo	ng L^{-1}	3.81 ± 0.15	10 [551]	14.7 ± 0.6	11 [3]	NA
dNi	ng L^{-1}	232 ± 7	6 [3]	381 ± 4	24 [35]	240 ± 12 – 376 ± 5 [1]
dCu	ng L^{-1}	85.4 ± 2.5	10 [551]	206 ± 3	24 [3]	115 ± 10 – 333.0 ± 0.7 [1]
dCd	ng L^{-1}	3.1 ± 0.7	8 [4]	52.2 ± 1.2	15 [667]	20.0 ± 0.5 – 49.0 ± 0.6 [1]
dPb	ng L^{-1}	0.99 ± 0.08	28 [186]	4.04 ± 0.13	10 [551]	0.52 – 6.0 [1]

Note. The measurement uncertainty of trace elements corresponds to twice the SD with µ ± 2σ. Literature data from Geotraces cruise GN02 in 2015 (station BB1, BB2 and BB3) and GreenEdge cruise in 2016 (stations G100 to G3000). [1](GEOTRACES Intermediate Data Product Group, 2023). [2](Bruyant et al., 2022). [3](Miller et al., 2020). [4](H. Thomas, personal communication, June 28, 2024).

https://doi.org/10.5194/egusphere-2025-291
Preprint. Discussion started: 11 February 2025

3.1 Basic oceanographic parameters

Because of the high resolution of the CTD data, we give ranges of minimum and maximum values for salinity, potential temperature, oxygen and AOU in Table S 5. Salinity values were the lowest in surface waters of stations close to the coast (stations 6, 11 and 17) and towards the west of each transect (stations 14, 15, 24, 29 and 30), ranging between 29.70 and 32.60. In the deep waters of station 10, the salinity was the highest with 34.88 over a depth range from 500 to 558 m. Minimum potential temperature values between -1.50 to -1.61°C were reached in the intermediate waters (20 to 75 m) of stations 24 and 30. Maximum potential temperature values between 5.6 to 6.7°C were measured in surface waters of transect 2 (stations 6, 7, 8 and 10), and in surface waters of station 17 in Disko Bay. Overall, temperatures were higher in the southeast of Davis Strait along the west Greenland coast and lower in the northwest of Davis Strait further offshore. In the deep waters of station 15, minimum oxygen concentrations between 203 to 210 µmol L^{-1} and maximum AOU values between 140 to 147 µmol L^{-1} were present over a depth range from 640 to 667 m. Maximum oxygen concentrations between 355 to 406 µmol L^{-1} and minimum AOU values between -26 to -72 µmol L^{-1} were measured in the photic zone (1.5 to 40 m) either close to the Greenlandic coast at the beginning of a transect (stations 6 and 17) or towards the west of each transect (stations 10, 14, 15 and 24).

3.2 Macronutrients

The overall nutrient distribution is shown as vertical profiles in Fig. S 6 and as sea surface concentration plots in Fig. S 7. In surface waters, nutrient concentrations were uniformly low across the shelf. Especially NOx (< LOQ = 0.21 µmol L^{-1}) was extremely low in surface waters and shallow shelf waters. Exceptions to this are surface waters with higher nutrient concentrations at station 17 in Disko Bay and at stations 14, 15, 24 and 30 toward the west of each transect. Below the biological productive zone, nutrient concentrations gradually increased with depth, reaching maximum concentrations at station 15 (667 m) (refer to Table 1).

In comparison to data collected during 2015 (GEOTRACES Intermediate Data Product Group, 2023) and 2016 (Bruyant et al., 2022), maximum nutrient concentrations of this study are lower, which we attribute to regional differences in the study areas, especially referring to the maximum sampling depth. We measured maximum values at the shelf edge at 667 m, whereas the references reported maximum values at stations more central to Baffin Bay in much greater depths.

3.3 Dissolved trace elements

The distributions of trace elements are shown as vertical profiles in Fig. S 8 and surface water concentrations in Fig. S 9. The vertical profiles of dV and dCu showed opposing trends (refer to Fig. S 8 a and f). With depth, dV concentrations increased, while dCu concentrations decreased. The dV concentrations ranged from 1270 ± 30 ng L^{-1} (station 24; 3 m) to 1810 ± 60 ng L^{-1} (station 10; 551 m), while dCu concentrations ranged from 206 ± 3 ng L^{-1} (station 24; 3 m) to 85.4 ± 2.5 ng L^{-1} (station 10; 551 m), both matching minimum and maximum occurrences of salinity. Surface waters close to the coast of Greenland and at the western end of each transect showed lower dV concentrations (Fig. S 9 a) and higher dCu concentrations (Fig. S 9 f),

https://doi.org/10.5194/egusphere-2025-291
Preprint. Discussion started: 11 February 2025

respectively. The distributions of dFe, dNi and dCd showed low concentrations in surface and subsurface waters, which gradually increased with depth (refer to Fig. S 8 c, e and g), reaching maximum concentrations for dFe of 630 ± 30 ng L^{-1} (station 18; 256 m), for dNi of 307 ± 9 ng L^{-1} (station 15; 667 m) and for dCd of 52.2 ± 1.2 ng L^{-1} (station 15; 667 m). Minimum concentrations of dFe, dNi and dCd were present in surface waters (refer to Table 1) of stations with some distance to the coast, with dFe concentrations below the LOQ (< 50 ng L^{-1}) at certain stations. The concentration of dFe and dNi in surface waters (Fig. S 9 c and e) followed a similar pattern as the surface water nutrient concentrations (Fig. S 7). The concentrations were higher close to the coast, decreased with distance along each transect and increased again towards the west of each transect. The surface water concentrations of dCd were rather uniform and increased only towards the west of each transect (Fig. S 9 g). The concentrations of dMn and dCo decreased from surface to subsurface waters and increased again with depth at stations located on the shelf (refer to Fig. S 8 b and d). On the shelf edge, concentrations of dMn and dCo remained stable with depth, leading to minimum concentrations for dMn of 54.8 ± 1.8 ng L^{-1} (station 24; 317 m) and for dCo of 3.81 ± 0.15 ng L^{-1} (station 10; 551 m). In surface waters, high concentrations of dMn and dCo were present at station 17 in Disko Bay and at stations 11 and 12, where the mouth of the Nassuttooq Fjord is located (Fig. S 9 b and d). The dMn and dCo concentrations in surface waters decreased with increasing distance from the coast. The depth profile of dPb does not follow a clear pattern (refer to Fig. S 8 h). South of Davis Strait, high dPb concentrations were observed across transect 2, alongside a maximum dPb concentration of 4.04 ± 0.13 ng L^{-1} in the deep waters of station 10. North of Davis Strait, dPb concentrations were below the LOQ (< 0.98 ng L^{-1}) in the deep waters of station 15, intermediate to deep waters of Disko Bay (stations 17 and 18) and in deep waters of station 28, along with a minimum concentration of 1.1 ± 0.4 ng L^{-1} in deep waters of station 30. In comparison to literature values, our results for trace element concentrations are in a similar range as data collected during the 2015 Geotraces cruise GN02 (GEOTRACES Intermediate Data Product Group, 2023). Variations of minimum and maximum values occur because of differences in sampling locations. While this study took place on the shelf, capturing the influence of coastal runoff as well as sea ice meltwater, the Geotraces cruise focused on stations off the shelf and further north in central Baffin Bay.

3.4 Carbonate system parameters

The vertical profiles of AT and CT (Fig. S 10 a and b) show a gradual increase with depth. Minimum concentrations of AT and CT were present in the low-salinity surface waters of station 15 (AT: 2062 µmol kg^{-1}; CT: 1949 µmol kg^{-1}). While maximum CT concentrations of 2214 µmol kg^{-1} were observed in the deep waters of station 15, AT concentrations followed the salinity gradient, reaching a maximum value of 2305 µmol kg^{-1} in the deep waters of station 10. The vertical profiles of pH and pCO_2 (Fig. S 10 d and e) show opposing trends, with pH increasing and pCO_2 decreasing towards intermediate waters of the photic zone. Below the photic zone, pH decreases and pCO_2 increases gradually with depth. This led to a pH maximum (8.20) and pCO_2 minimum (249 µatm) in the photic zone of station 15 at 32 m, as well as minimum pH values of 7.86 and maximum pCO_2 values of 559 µatm in the deep waters of station 15. The vertical profiles of the CT:AT ratio, the Revelle factor and Ω Aragonite (Fig. S 10 c, f and g) show that these parameters remain relatively stable in the first 25 m of the water

https://doi.org/10.5194/egusphere-2025-291
Preprint. Discussion started: 11 February 2025

column and gradually increase (CT:AT ratio and Revelle factor) or decrease (Ω Aragonite). In the surface waters of Disko Bay (station 17; 3 m) a minimum CT:AT ratio of 0.907, together with a minimum Revelle factor of 11.85 and a maximum Ω Aragonite value of 2.17 were present. The maximum CT:AT ratio (0.968) was found in the deep waters of station 15, which coincides with a maximum Revelle factor of 17.80 and a minimum Ω Aragonite value of 0.90. The surface water concentrations of the carbonate system parameters are given in Fig. S 11. In general, stations closest to the coast of Greenland showed lower AT and CT values that increased with distance to the coast. Following this trend, the pH in surface waters increased and pCO_2 values decreased with distance to the coast along each transect. The lower CT:AT ratios of coastal stations coincided with higher Revelle factors and lower Ω Aragonite values, reflecting the lower buffering capacity of coastal waters. An exception to this was the surface waters of Disko Bay (station 17; 3 m). Here, the CT:AT ratio reached a minimum (0.907), caused by low CT values of 1972 µmol kg^{-1}, corresponding to low pCO_2 values of 255 µatm. Coupled to this, the pH is high (8.19) and the Revelle factor low (11.85), indicating the higher buffering capacity of this water, which is also reflected by a maximum Ω Aragonite value of 2.17. The westernmost surface waters of each transect showed lower AT and CT values with overall highest CT:AT ratios in surface waters. Consequently, pCO_2 values and Revelle factors followed this trend and were higher at these stations, whereas pH and Ω Aragonite values were lower.

In comparison to AT and CT data collected during 2015 (H. Thomas, personal communication, June 28, 2024) and 2016 (Miller et al., 2020), our results are in a similar range as previous studies, but with minimum values being slightly lower as we were able to capture the sea ice meltwater signal.

4 Discussion

4.1 Characterization of water masses

4.1.1 Temperature-salinity properties

The water masses along the west Greenland shelf were identified using salinity and potential temperature (Curry et al., 2014; Tang et al., 2004; Curry et al., 2011; Sherwood et al., 2021) as shown in Fig. 2. Water depth profiles displaying potential temperature, salinity, potential density, and oxygen along the transects are provided in Fig. S1 to S5. The West Greenland Shelf Water (WGSW; $\Theta < 7$°C; S < 34.1) was the dominant water mass in the study area, occurring in each transect across the shelf above a water depth of 200 m. The West Greenland Intermediate Water (WGIW; $\Theta > 2$°C; S > 34.1) was present in deeper waters along the slope below 200 m. Arctic Water (AW; $\Theta \leq 2$°C; S ≤ 33.7) was encountered north of Davis Strait at transects 3, 4, and 5 as an interlayer between WGSW and WGIW above 100 m on the west side of the transects, forming cold and low-salinity pockets of water (Fig. S 3 to S 5). At transect 4, AW was found at station 17 approximately 70 km off the coast of Greenland, reaching far into Disko Bay. Transitional Water (TrW; $\Theta \leq 2$°C; S > 33.7) was present mainly at transects 4 and 5 between 100 and 200 m, separating AW from WGIW (Fig. S 4 to S 5). At station 15, the waters below 300 m were defined as Baffin Bay Water (BBW; $\Theta \leq 2$, S > 34.1), a shallower extension of the Baffin Bay Deep Water, presenting as a

https://doi.org/10.5194/egusphere-2025-291
Preprint. Discussion started: 11 February 2025

295 distinct tail on the Θ-S diagram (Sherwood et al., 2021). Due to very low surface salinity values at stations 14, 15, and 24 (S < 31.5), we introduced sea ice meltwater (SIM) as an additional source water to distinguish areas affected by sea ice melt.

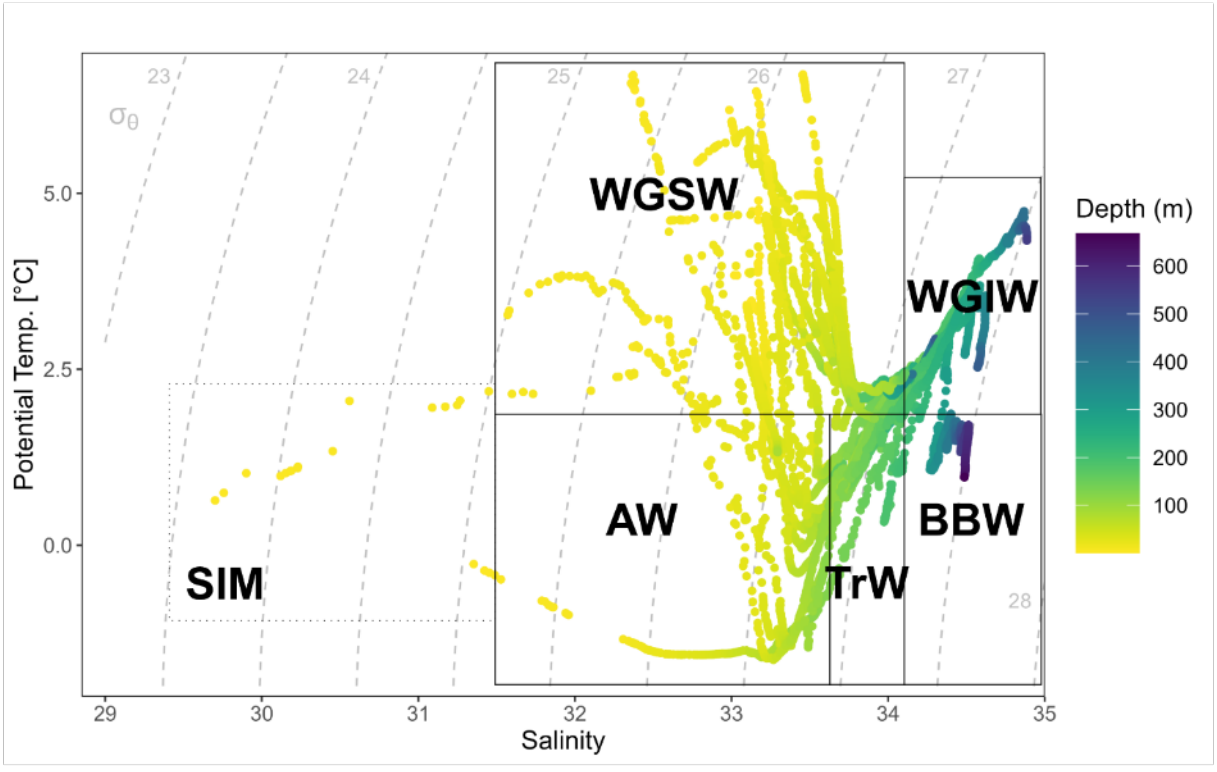

Figure 2: Water masses in the study area were characterized using potential temperature and salinity: West Greenland Shelf Water (WGSW; Θ < 7°C; S < 34.1), West Greenland Intermediate Water (WGIW; Θ > 2°C; S > 34.1), Transitional Water (TrW; Θ ≤ 2°C;
300 **S > 33.7), Arctic Water (AW; Θ ≤ 2°C; S ≤ 33.7) and Baffin Bay Water (BBW; Θ ≤ 2, S > 34.1), according to Curry *et al.* (2011), Curry *et al.* (2014), Sherwood *et al.* (2021), and Tang *et al.* (2004). Surface water with S < 31.5 is indicative of sea ice meltwater (SIM).**

4.1.2 Influence of physicochemical processes on biogeochemical properties

The extensive data set was processed using PCA to further characterize the water masses and to find physicochemical processes
305 that alter the distribution of carbon, macronutrients, and trace elements. The results of the PCA analysis are summarized in Table S 6, with significant PC loadings of each parameter marked in bold. Overall, 82 % of the total variance in the normalized data set can be explained by three PCs. The majority of variance is explained by PC 1 with 52 %, followed by PC 2 with 18 % and PC 3 with 12 %. Salinity, depth, oxygen, AT, CT, dV, and dCu significantly load on PC 1; potential temperature, AOU, NOx, silicate, phosphate, dNi, dCd, and dPb significantly load on PC 2; and dFe, dMn, dCo, dNi, and dCu significantly load
310 on PC 3. Figure 3 shows the results of the PCA as biplots with colors indicating the water mass affiliation of each sample.

https://doi.org/10.5194/egusphere-2025-291
Preprint. Discussion started: 11 February 2025

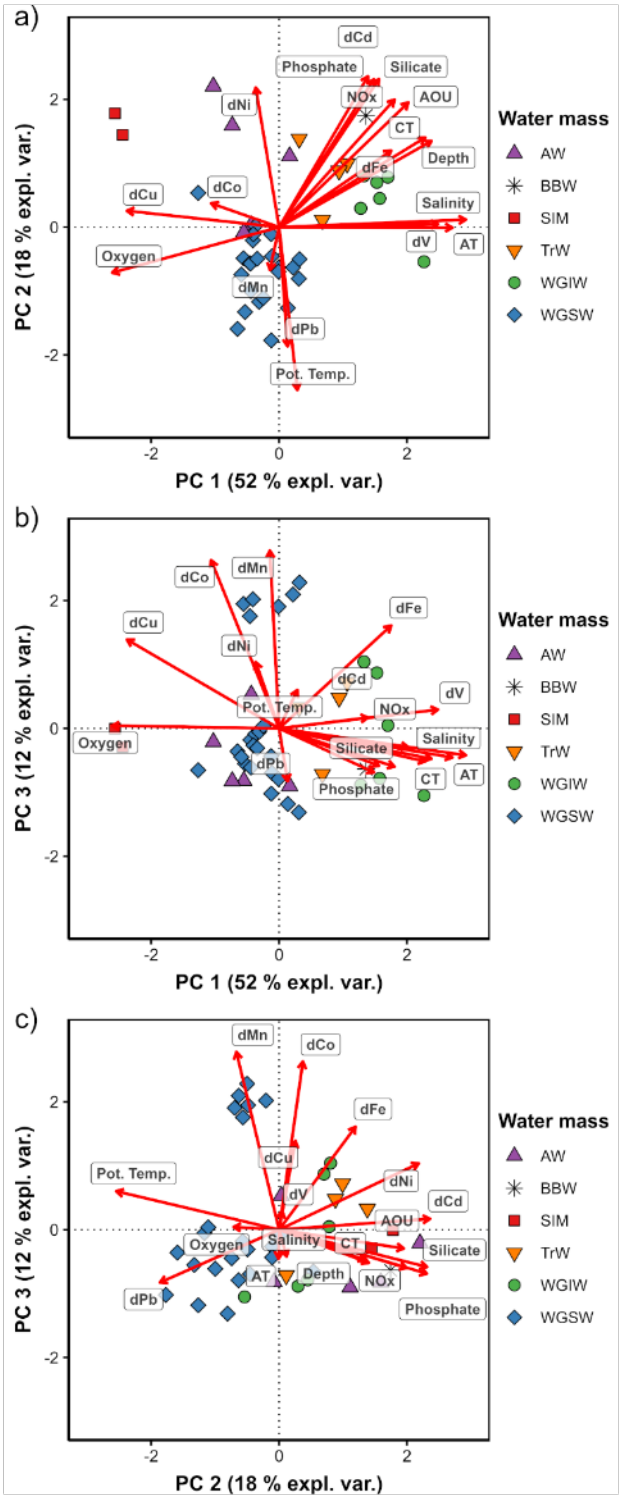

Figure 3: Biplots according to PCA results for a) PC 1 score vs PC 2 score; b) PC 1 score vs PC 3 score; and c) PC 2 score vs PC 3 score, with colors indicating the water mass affiliation of each sample. The loading of each parameter is indicated by a red arrow.

https://doi.org/10.5194/egusphere-2025-291
Preprint. Discussion started: 11 February 2025

Conservative mixing along the salinity gradient (PC 1)

The comparison of low PC 1 scores of surface water samples with lower salinity (WGSW, AW, and SIM) and high PC 1 scores of deep water samples with higher salinity (WGIW, TrW, and BBW) indicates that PC 1 is resolving the salinity gradient of the study area (Fig. 3 a and b). The WGSW integrates freshwater contributions from the GIS (Foukal and Pickart, 2023), while AW mixes winter-cooled water entering Baffin Bay on the eastern side of Davis Strait with inflow of cold and fresh Arctic Ocean water of Pacific origin through the CAA (Curry et al., 2014). Melt water from sea ice promotes a fresh surface layer that tends to remain concentrated in the upper part of the water column (Haine et al., 2015). The statistical results illustrate the importance of freshwater input on the chemical properties of the study area. The high loading of AT, CT, dV, and dCu on PC 1 indicates that these parameters behave conservatively, with freshwater either being a source (dCu) or a cause for dilution (AT, CT, and dV) of parameter concentrations. The positive loadings of AT and CT on PC 1 are in line with the general understanding of freshwater inputs from sea ice meltwater and glacial meltwater, which are characterized by low AT and CT values (Bates and Mathis, 2009; Chierici and Fransson, 2009; Fransson et al., 2015). The positive correlation of AT and CT are illustrated in Fig. S 12 a and b. The distribution of dV shows a positive correlation with salinity (Fig. S 12 c) as both sea ice melt and coastal freshwater inputs were characterized by low dV concentrations (Marsay et al., 2018; Whitmore et al., 2019). The distribution of dCu correlated negatively with salinity and was influenced by coastal freshwater input and sea ice meltwater as a dCu source (Fig. S 12 d). Cu-binding ligands play an important role in maintaining Cu in the dissolved phase (Ruacho et al., 2022) and facilitate the transport of dCu across the Arctic (Arnone et al., 2023). This is reflected in the consistent decrease of dCu concentrations in the lateral direction away from the coastal source along the shelf transects (refer to Sect. 3.3). The influence of freshwater input on the chemical properties of the water column is further discussed regarding sea ice meltwater in Sect. 4.4 and coastal runoff in Sect. 4.5.

Biological uptake and recycling (PC 2)

The high positive loading of AOU, NOx, silicate, phosphate, dNi, and dCd on PC 2 suggests that PC 2 describes distributions that are controlled by biological cycling. The nutrient-type behavior of dNi and dCd was mentioned in Sect. 3.3 and agrees well with the PCA results. In addition, dFe shows high loadings on PC 2, reflecting its nutrient-type character. This in good agreement with previously published data for the Nansen Basin and the Barents Sea (Gerringa et al., 2021), the Chukchi Sea (Vieira et al., 2019), the Fram Strait (Krisch et al., 2022a) and the Canadian Arctic (Colombo et al., 2020). The anticorrelation of nutrients (positive PC 2 loading) and potential temperature (negative PC 2 loading) derives from the distribution of those parameters across the study area. The low PC 2 scores of WGSW indicate that the warmer shelf waters are highly productive, resulting in low nutrient concentrations. The colder deep waters of TrW, WGIW and BBW are characterized by high PC 2 scores which implies that remineralization occurred with nutrients and trace elements being returned to the water column. Similarly, water samples of AW and SIM show high PC 2 scores with higher nutrient concentrations alongside colder

https://doi.org/10.5194/egusphere-2025-291
Preprint. Discussion started: 11 February 2025

temperatures. The difference in nutrient concentrations between AW and WGSW is further discussed in Sect. 4.3 and the influence of the retreating sea ice in Sect. 4.4.

The remineralization of organic matter (OM) led to elevated concentrations of NOx, silicate, phosphate, and dCd, together with maximum AOU values (refer to Sect. 3.1 and 3.2) in the deep waters of BBW (640 to 667 m; station 15). Although we only encountered BBW at this station, our results agree well with Sherwood *et al.* (2021), who observed a similar trend with similar AOU and nutrient concentrations in BBW. Remineralized nutrients accumulate at depth because of the long residence time of deep and bottom waters in Baffin Bay in combination with an enclosed bathymetry that restricts circulation (Sherwood et al., 2021; Lehmann et al., 2019). Besides nutrients, CT also has a high loading on PC 2, while AT only loads on PC 1. This statistical feature illustrates the different biogeochemical behavior of AT and CT. While AT distributions are dominated by freshwater dynamics, CT distributions are also equally driven by biological processes. This resulted in elevated CT concentrations in BBW (refer to Sect. 3.4). Here, high CT values coincided with the restricted circulation, which led to overall more corrosive conditions for the Baffin Bay shelf sediments and benthic ecosystem. Similar to other studies of Baffin Bay (Beaupré-Laperrière et al., 2020; Burgers et al., 2024), respiration of OM drove deep waters to become undersaturated with respect to Ω Aragonite, with pCO_2 increasing and pH decreasing proportionally to each other (refer to Sect. 3.4).

Alongside potential temperature, dPb has a negative loading on PC 2, which stems from the latitudinal trend of potential temperature and dPb concentrations (refer to Sect. 3.1 and 3.3). The distribution of dPb is mainly controlled by the mixing of warm Atlantic-origin waters with high dPb signatures and cold Arctic-origin waters with low dPb signatures (Colombo et al., 2019). This resulted in high dPb concentrations in the warmer waters southeast of Davis Strait, which decreased towards the northwest as temperatures decreased.

Scavenging and benthic processes (PC 3)

The third PC associates with the trace elements dMn, dFe, dCo, dNi, and dCu. It is known that during estuarine mixing, dCo, dNi and dCu are co-cycled with dMn and dFe during their transformation into the respective (oxy)hydroxide minerals (Smrzka et al., 2019). We suggest that PC 3 indicates particle-driven mixing of these trace elements with coastal runoff as a source. High PC 3 scores (Fig. 3 b and c) of surface samples taken at stations 11 and 12 (mouth of Nassuttooq Fjord) as well as station 17 (Disko Bay) illustrate the prevailing role of coastal freshwater inputs on the distribution of these trace elements. The influence of coastal runoff on trace element distribution is further discussed in Sect. 4.5.

The biplots (Fig. 3 b and c) reveal an interesting feature of deep water samples (111 to 667 m), identified as TrW and WGIW. At these shelf stations, deep water concentrations of dMn, dFe, dCo, and dNi are increased (refer to Sect. 3.2), which we suggest is caused by benthic processes in surface sediments, i.e., reversible scavenging linked to mineral dissolution and remineralization of organic material. Release from the benthic boundary layer has been described for dCo, dFe, and dMn in the Barents Sea (Gerringa et al., 2021), the Chukchi Sea (Vieira et al., 2019), the Canadian Arctic (Colombo et al., 2020) and throughout the Arctic basin (Bundy et al., 2020) and for dNi in the Bering Sea and Chukchi Sea (Jensen et al., 2022). In contrast, dCu showed no benthic source or evidence of biological cycling and instead remained dominated by freshwater runoff

https://doi.org/10.5194/egusphere-2025-291
Preprint. Discussion started: 11 February 2025

from coastal sources, similar to what has been observed by Jensen *et al.* (2022). Noticeable for these deep water shelf samples is a dissociation of corresponding PC 3 scores into negative scores (stations 8, 10, 15, 24, 30) and positive scores (stations 17, 20, 22, 28). We believe this division to be caused by differences in return fluxes at the sediment-water interface. Stations with a positive PC 3 score are closer to the coast, where more biogenic and terrigenous material is exported, which can be recycled in deep waters. Stations that are further away from the coast do not receive as much material for remineralization and have, thus, a negative PC 3 score with lower concentrations of the trace elements dMn, dFe, dCo and dNi. A similar observation was made for dMn, dFe, and dCo in the Ulleung Basin of the East Sea by Seo *et al.* (2022). Concentrations were significantly higher on the slopes and bottom layer of the Ulleung Basin in contrast to the Japan Basin, which the authors associated with a large sedimentary release by OM degradation caused by the high OM content of the shelf sediments (Seo et al., 2022).

4.3 Influence of major current systems on biogeochemical properties

The spatial distribution of parameters revealed significant differences in eastern and western shelf waters. We decided to directly compare the three major water masses present along the west Greenland shelf: the northward-moving WGSW (1 to 220 m) and WGIW (130 to 560 m) with the southward-moving AW (2 to 165 m). For each parameter, the median and the mean ± SD values are summarized in Table 2. The median is used throughout the data discussion because of its robustness against outliers.

https://doi.org/10.5194/egusphere-2025-291
Preprint. Discussion started: 11 February 2025

395 **Table 2: Comparison of the median and mean ± SD concentrations between WGSW, WGIW and AW. The number of samples (*n*) used for the calculation is given in brackets.**

	Parameter	WGSW (Median; Mean ± SD)	WGIW (Median; Mean ± SD)	AW (Median; Mean ± SD)
Basic oceanographic parameters (WGSW: $n = 3021$; WGIW: $n = 3034$; AW: $n = 2301$)	Salinity	33.57	34.45	33.48
		33.52 ± 0.42	34.45 ± 0.23	33.42 ± 0.27
	Pot. Temp. (°C)	2.68	2.93	0.38
		3.20 ± 1.15	3.16 ± 0.73	0.15 ± 1.02
	Oxygen ($\mu mol\ L^{-1}$)	336	273	332
		344 ± 23	278 ± 21	332 ± 23
	AOU ($\mu mol\ L^{-1}$)	-4	62	36
		0 ± 26	55 ± 23	30 ± 24
Macronutrients (WGSW: $n = 54$; WGIW: $n = 9$; AW: $n = 29$)	NOx ($\mu mol\ L^{-1}$)	1.7	13.5	5.7
		2.4 ± 2.8	13.7 ± 1.7	6.0 ± 2.8
	Silicate ($\mu mol\ L^{-1}$)	1.5	10.6	4.2
		2.0 ± 1.8	11.5 ± 4.1	5.2 ± 3.5
	Phosphate ($\mu mol\ L^{-1}$)	0.23	1.02	0.66
		0.31 ± 0.18	0.99 ± 0.13	0.68 ± 0.21
Carbonate system parameters (WGSW: $n = 50$; WGIW: $n = 12$; AW: $n = 25$)	AT ($\mu mol\ kg^{-1}$)	2226	2275	2237
		2228 ± 19	2278 ± 11	2237 ± 6
	CT ($\mu mol\ kg^{-1}$)	2051	2164	2104
		2056 ± 28	2159 ± 16	2104 ± 27
	CT:AT	0.922	0.950	0.941
		0.923 ± 0.007	0.948 ± 0.006	0.941 ± 0.010
	pH	8.14	7.99	8.10
		8.14 ± 0.03	7.99 ± 0.04	8.09 ± 0.06
	pCO_2 (µatm)	292	433	321
		295 ± 22	425 ± 37	332 ± 52
	Ω Aragonite	1.88	1.30	1.48
		1.86 ± 0.15	1.34 ± 0.12	1.49 ± 0.20

https://doi.org/10.5194/egusphere-2025-291
Preprint. Discussion started: 11 February 2025

Continuation of Table 2: Comparison of the median and mean ± SD concentrations between WGSW, WGIW and AW. The number of samples (*n*) used for the calculation is given in brackets.

	Parameter	WGSW (Median; Mean ± SD)	WGIW (Median; Mean ± SD)	AW (Median; Mean ± SD)
Trace elements (WGSW: $n = 31$; WGIW: $n = 8$; AW: $n = 8$)	dV (ng L^{-1})	1490	1735	1480
		1486 ± 234	1713 ± 121	1478 ± 127
	dFe (ng L^{-1})	116	262	162
		138 ± 67	329 ± 55	174 ± 26
	dMn (ng L^{-1})	237	89	186
		261 ± 71	164 ± 13	184 ± 20
	dCo (ng L^{-1})	8.0	5.0	9.0
		8.5 ± 2.5	5.7 ± 0.5	9.2 ± 0.8
	dNi (ng L^{-1})	254	269	266
		258 ± 51	270 ± 22	280 ± 20
	dCu (ng L^{-1})	161	111	160
		158 ± 44	111 ± 13	162 ± 16
	dCd (ng L^{-1})	13	31.6	21.6
		13 ± 6	32.2 ± 2.7	22.0 ± 2.3
	dPb (ng L^{-1})	2.4	2.4	1.7
		2.5 ± 0.8	2.4 ± 0.5	1.8 ± 0.4

The median values of salinity and potential temperature reflect the origin of the water masses and the freshwater dynamics of this area. In the upper water column, AW is slightly fresher (33.48) and colder (0.38°C) than WGSW (33.57; 2.68°C). This east–west gradient in temperature and salinity was also described by Tang *et al.* (2004) between Baffin Island and the Greenland coast. When the warmer WGSW flows cyclonically around Baffin Bay and mixes with adjacent water of the CAA, the water becomes colder and fresher before returning as the southward AW current (Tang et al., 2004). The WGIW is part of the deep water WGSC that transports warm (2.93°C) and salty (34.45) waters from the North Atlantic (Curry et al., 2014).

The AOU concentrations are reflective of respiration and the biological activity of the water (Sarmiento and Gruber, 2006). Lower AOU values in WGSW (-4 µmol L^{-1}) than in AW (36 µmol L^{-1}) indicate that the warmer shelf waters are more productive than the colder AW. This is also in agreement with overall lower nutrient concentrations in WGSW than AW (refer to Sect. 4.1.2 and Table 2), as nutrients are removed from the water column through PP. With depth, respiration returns nutrients to the water column as seen by high AOU values in WGIW (62 µmol L^{-1}) and overall higher nutrient concentrations (refer to Table 2). Fig. 4 a shows the NOx concentrations against longitude in a depth range of 30 to 50 m, including literature

https://doi.org/10.5194/egusphere-2025-291
Preprint. Discussion started: 11 February 2025

415 data from the Green Edge cruise in 2016 (Bruyant et al., 2022). There is a clear difference between lower NOx concentrations in WGSW on the shelf and higher NOx concentrations in AW further offshore in areas that were still ice-covered. This gradient in nutrient concentrations is caused by the direction of the sea ice retreat from east to west and has been linked to higher productivity and species richness along the southern coast of west Greenland and in Disko Bay, compared to Baffin Island and northwest Greenland (Krawczyk et al., 2021; Lafond et al., 2019). We believe that our sampling near the end of the summer
420 season was crucial for this vast difference in water mass composition. Shelf waters had already become depleted in nutrients, while further offshore biological processes only increased recently because of the retreating sea ice (refer to Sect. 4.4).

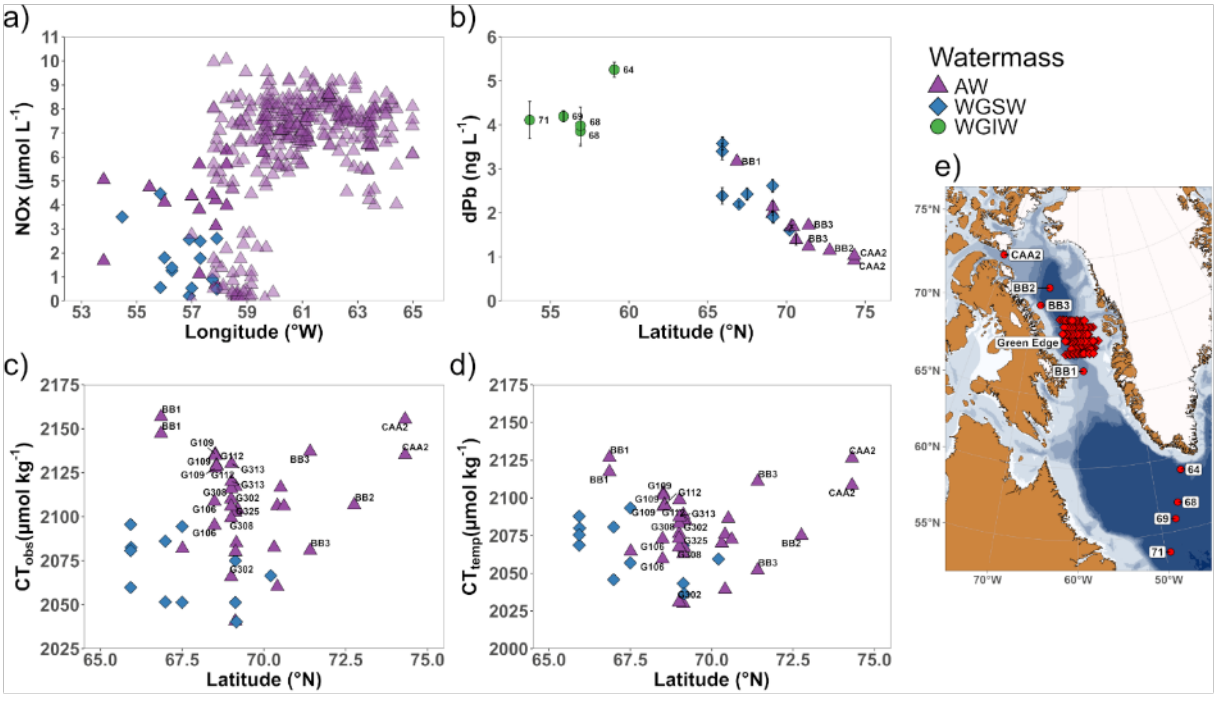

Figure 4: a) NOx vs. longitude between 30 and 50 m with results of this study in solid colors and results of the Green Edge cruise in
425 **transparent colors (Bruyant et al., 2022); b) dPb vs. latitude between 30 and 50 m with results of this study (unlabeled) in comparison to results of the Geotraces GA01 cruise in 2014 (stations 64-71) and Geotraces GN02 in 2015 (BB1-BB3, CAA2), both: (GEOTRACES Intermediate Data Product Group, 2023); c) CT_{obs} and d) CT_{temp} vs. latitude between 30 and 50 m with results of this study (unlabeled) in comparison to results of the Green Edge cruise (Miller et al., 2020) and Geotraces GN02 in 2015 (BB1-BB3, CAA2) (H. Thomas, personal communication, June 28, 2024); e) location of the stations used as comparison. Different water mass**
430 **categories are given in the legend.**

Comparison of the carbonate system parameters in WGSW and AW shows that both AT and CT median concentrations were lower in WGSW. This coincides well with a study by Burgers *et al.* (2024), which described the dominant source of freshwater for eastern Baffin Bay to be glacial meltwater with a much lower AT endmember (390 ± 140 µmol kg^{-1}) compared to the western Baffin Bay with an AT endmember of 1170 ± 120 µmol kg^{-1}. The higher median CT:AT ratios in AW (0.941)
435 compared to WGSW (0.922) are caused by the inflow of relatively low salinity Pacific waters to western Baffin Bay with higher CT:AT ratios, while Atlantic waters with low CT:AT ratios are transported to eastern Baffin Bay (Burgers et al., 2024).

https://doi.org/10.5194/egusphere-2025-291
Preprint. Discussion started: 11 February 2025

This carbon enrichment in AW can be traced back to the CAA outflow, which contains higher CT concentrations of Pacific-origin (Shadwick et al., 2011b; Azetsu-Scott et al., 2010). The slightly higher CT:AT ratios in AW than WGSW were also reflected by a higher median pCO_2 concentration and lower median pH value and median Ω Aragonite concentration (refer to Table 2). For a more detailed discussion about CT values in AW and WGSW, we looked at a depth range of 30 to 50 m to eliminate any depth dependency. It is known that colder sea surface temperatures at high latitudes explain the majority of the surface CT latitudinal gradient due to the increased CO_2 solubility of colder waters (Wu et al., 2019; Li and Tsui, 1971). We examined the extent of the CT change induced by the temperature difference between AW and WGSW. Therefore, we calculated temperature-normalized CT (CT_{temp}) according to Wu *et al.* (2019) (refer to Sect. 2.4.) based on the median potential temperature of WGSW (3.23°C) within a depth range of 30 to 50 m. The observed CT (CT_{obs}) and CT_{temp} values are shown in Fig. 4 c and d for AW and WGSW. We included literature data from the Green Edge cruise (Miller et al., 2020) and Geotraces GN02 in 2015 (BB1-BB3, CAA2) (H. Thomas, personal communication, June 28, 2024), filtered for a depth range of 30 to 50 m. Including literature data, the difference between the median CT values of AW and WGSW is $\Delta CT = 35$ µmol kg^{-1}. After temperature normalization, the difference is significantly reduced to $\Delta CT_{temp} = 12$ µmol kg^{-1}. Therefore, we conclude that most of the CT difference in AW and WGSW is induced by the temperature difference of both water masses. The remaining CT difference could be caused by the higher productivity in WGSW, which lowers CT concentrations, combined with the mixing of AW and the CAA outflow, which is known to transport additional CT to Baffin Bay (Shadwick et al., 2011b; Burgers et al., 2024; Azetsu-Scott et al., 2010). Towards the deeper water of WGIW, AT and CT median concentrations were higher as they increased along the salinity gradient and respiration of OM released CT to the water column. This is also reflected in higher median pCO_2 concentrations and lower median Ω Aragonite concentrations in WGIW (refer to Table 2), similar to observations by Burgers *et al.* (2024).

All median concentrations of trace elements that showed a nutrient-type profile (dFe, dNi, and dCd) are lower in WGSW than AW. This difference is caused by their uptake during PP, which was higher in WGSW than AW. The return of these elements to the water column due to remineralization of OM can be seen in higher median concentrations in WGIW (refer to Table 2). Furthermore, variations in source water concentrations could lead to differences in trace element concentrations. AW showed elevated concentrations for dFe, dMn, dCo, dNi, and (refer to Table 2). We attribute these high concentrations to the CAA outflow into Baffin Bay, which was found to have higher dFe and dMn concentrations caused by sediment resuspension in the benthic boundary layer (Colombo et al., 2020; Colombo et al., 2021), as well as higher dNi and dCu concentrations due to waters advected from the Canada Basin through the CAA and out into Baffin Bay (Jensen et al., 2022). In contrast, higher dPb median concentrations were present in WGSW and WGIW than AW (refer to Table 2). As mentioned in Sect. 3.3, there is a difference in dPb concentrations between the south and the north of Davis Strait, with dPb concentrations decreasing along the west coast of Greenland. We illustrated this trend by plotting dPb against latitude in a depth range between 30 and 50 m (Fig. 4 b) as a combination of our results with literature data from the Geotraces GA01 cruise in 2014 (stations 64 to 71) and Geotraces GN02 in 2015 (BB1-BB3, CAA2), both: (GEOTRACES Intermediate Data Product Group, 2023). The results show that WGSW and WGIW entailed higher dPb concentrations, with freshwater from the GIS (Krisch et al., 2022b) and water

https://doi.org/10.5194/egusphere-2025-291
Preprint. Discussion started: 11 February 2025

from the North Atlantic (Colombo et al., 2019) being as a source of dPb, respectively. In contrast, AW contained much lower dPb concentrations, which we relate to low dPb concentrations in the CAA outflow as this region is relatively remote from anthropogenic inputs (Colombo et al., 2019). Our results demonstrate that the distribution of dPb is mainly controlled by the mixing of water masses with different dPb signatures and can be used to illustrate the gradual mixing of the three water masses along the shelf.

4.4 Influence of retreating sea ice on biogeochemical properties

Baffin Bay and its surrounding areas are generally ice-free between July and October (Bi et al., 2019). The statistical analysis illustrated the importance of SIM on the chemical composition of surface waters (refer to Sect. 4.1.2). We used the ASI sea ice concentration product provided by the University of Bremen (Spreen et al., 2008) to visualize the decline in sea ice concentration over the sampling period. Figure 5 a shows the difference in sea ice concentration between 19 July and 28 July 2021. At the beginning of our sampling period on 19 July 2021, two large areas with high sea ice concentration were present between 66°N-68°N and 70°N-74°N. These areas had disappeared almost completely by the end of our sampling period on 28 July 2021, indicating the complete melting of sea ice in the study area over 10 days. The melt event affected sea surface salinity and potential temperature, depicted in Fig. 5 b and c. Both parameters decrease towards west along transects 3, 4 and 5 with salinity reaching a minimum of 29.70 (station 14; 3 m) and potential temperature of -0.36°C (station 24; 3 m). The category SIM (refer to Sect. 4.1) was identified in the top 4 m of stations 14 and 24 and in the top 8 m of station 15. Although not identified as SIM, a similar trend of decreasing surface salinity and potential temperature values can be seen at stations 10, 13, 23, 28, 29, and 30, adjacent to SIM stations (Fig. S 2 to S 5). We suggest that this trend is caused by the gradual advection of SIM from Baffin Bay towards the southeast.

https://doi.org/10.5194/egusphere-2025-291
Preprint. Discussion started: 11 February 2025

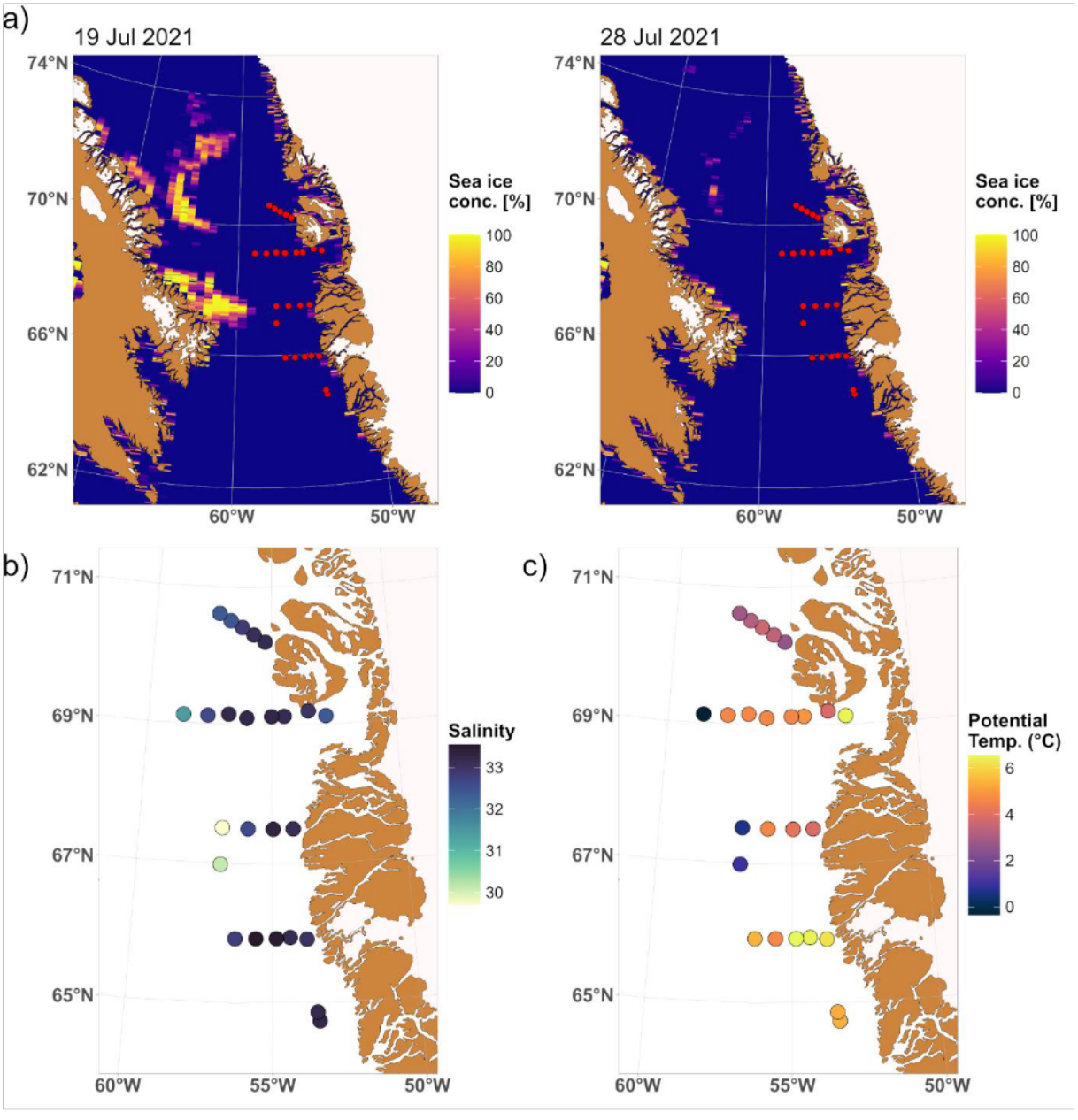

Figure 5: a) Sea ice concentration (%) in the study area during the sampling period on 19 July and 28 July 2021. Sea ice concentration data (ASI data, ASMR2, version 5.4, 3.125 km grid) was downloaded from the data archive of the University of Bremen (Spreen et al., 2008). Sea surface b) salinity and c) potential temperature from CTD sensor data.

Lafond *et al.* (2019) observed that stations covered by sea ice had higher surface nutrient concentrations than open-water stations located east of the ice edge, where nutrients were close to depletion. In this study, the distribution of nutrients in surface waters follows a similar trend (refer to Sect. 3.2). Along each transect, nutrient concentrations were higher towards the west, following the retreat of the sea ice. High oxygen and low AOU values in these areas (refer to Sect. 3.1) suggest that a

https://doi.org/10.5194/egusphere-2025-291
Preprint. Discussion started: 11 February 2025

phytoplankton bloom started to develop. The timing of the study enabled us to observe that nutrients had not yet been consumed in these western areas, whereas shelf waters had already become depleted towards the east.

Our observations of the carbonate system show that surface waters of stations affected by SIM had lower AT and CT concentrations, with overall higher CT:AT ratios, resulting in higher pCO_2 values and lower Ω Aragonite values (refer to Sect. 3.4). Similar results of sea ice meltwater increasing pCO_2 and decreasing $CaCO_3$ mineral saturation states have been described along the east and west coast of Greenland (Henson et al., 2023), the Fram Strait (Tynan et al., 2016) but also in other parts of the Arctic such as the Canada Basin (Bates et al., 2009). To investigate the effect of sea ice on the first 50 m of the water column, which is the penetration depth of sea ice meltwater (Jones et al., 1983), we calculated salinity-normalized AT ($AT_{sal} = 35AT/S$) and temperature-salinity-normalized CT ($CT^{sal}_{temp} = 35CT_{temp}/S$) according to Wu *et al.* (2019) (refer to Sect. 2.4. and 4.3). We used normalized concentrations to account for temperature and salinity effects on the solubility of CO_2. The normalized concentrations remain dependent on biological processes, air–sea gas exchange and mixing of water masses (Shadwick et al., 2011a). For AT_{sal} (Fig. 6 a), the majority of surface water concentrations range between 2330 and 2350 µmol kg^{-1}. We observed an addition in AT of ≈ 25 to 55 µmol kg^{-1} for SIM stations and of ≈ 5 to 45 µmol kg^{-1} for SIM adjacent stations. Our results agree well with Jones *et al.* (1983), who observed an AT addition of ≈ 100 µmol kg^{-1} further north in Baffin Bay, in a region that is more dominated by sea ice meltwater than our study area. The additional AT is released during melting of sea ice containing ikaite (Rysgaard et al., 2012; Rysgaard et al., 2011; Jones et al., 1983). The expected change in CT by ikaite dissolution should be one-half the corresponding change in AT (Jones et al., 1983), or approximately 15 to 30 µmol kg^{-1}. The CT^{sal}_{temp} values are shown in Fig. 6 b with most surface water concentrations ranging between 2140 and 2170 µmol kg^{-1}. There is an addition in CT^{sal}_{temp} for SIM stations of ≈ 60 to 75 µmol kg^{-1} and of ≈ 10 to 60 µmol kg^{-1} for SIM adjacent stations. Hence, the observed CT addition is much higher than what is expected from ikaite dissolution alone. Possible explanations for this high surplus in CT could be the release of CT derived from organic carbon remineralization under the ice (Tynan et al., 2016; Bates et al., 2009) and the inflow of additional CT transported through the CAA to Baffin Bay (Shadwick et al., 2011b; Henson et al., 2023; Azetsu-Scott et al., 2010). Our results show that the dissolution of ikaite in sea ice acted as a source of AT, providing a small geochemical buffer to meltwater-influenced surface waters (Jones et al., 2021). However, the inflow of Pacific-origin waters and remineralization under the ice led to overall higher CT:AT ratios, resulting in higher pCO_2 and lower pH and Ω Aragonite values in surface waters. There is evidence that once the sea ice melt facilitated bloom fully develops and CT is removed by PP from seawater, higher pH and Ω Aragonite values can be expected along the sea ice edge (Tynan et al., 2016). This can be seen in the photic zone of station 15 at 32 m, where an oxygen maximum (and AOU minimum) was present, which indicates high PP, resulting in a pH maximum (8.20) and pCO_2 minimum (249 µatm) (refer to Sect. 3.4).

https://doi.org/10.5194/egusphere-2025-291
Preprint. Discussion started: 11 February 2025

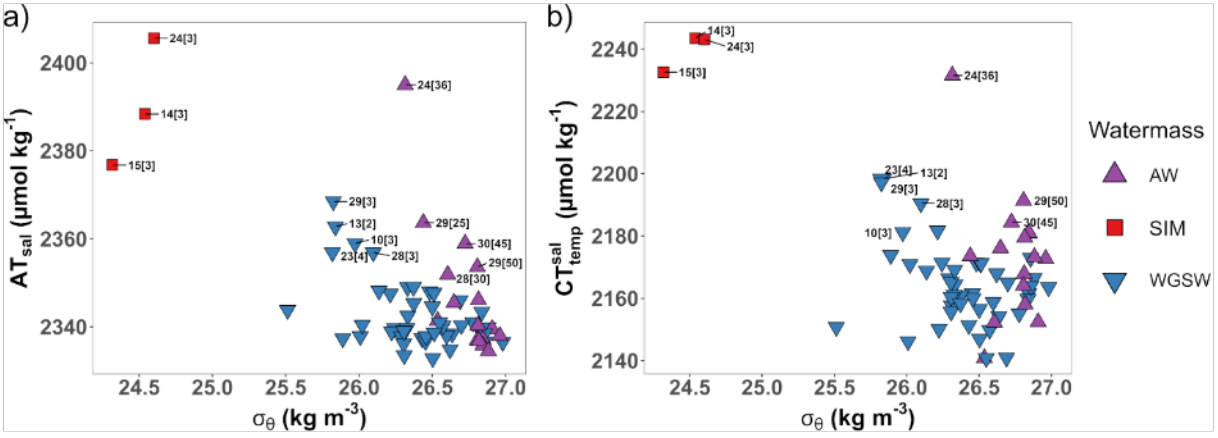

Figure 6: First 50 m of the water column for a) salinity-normalized AT values against pot. density and b) temperature-salinity-normalized CT values against pot. density. Different water mass categories are given in the legend. SIM affected stations (14, 15, 24) and stations adjacent to those (10, 13, 23, 28, 29, 30) are labeled. The number in brackets corresponds to the sampling depth.

We observed higher surface water concentrations of dFe, dCo, dNi, dCu, and dCd in areas that were recently covered by sea ice towards the west of each transect (refer to Sect. 3.3). This ties in nicely with a study by Tovar-Sánchez *et al.* (2010), who observed these trace elements to be enriched in sea ice relative to surface waters, suggesting that sea ice meltwater is a significant source of these trace elements to Baffin Bay surface waters. Especially, the additional input of dFe from melting sea ice could be biologically important in maintaining ice-edge blooms, as seen, e.g., in the Bering Sea (Aguilar-Islas et al., 2008). Besides the additional input through sea ice meltwater, we suggest that much like macronutrients, trace elements have not yet been removed from surface waters by biological uptake. We hypothesize that after the occurrence of the bloom, both macronutrient as well as trace element concentrations would decrease, much like we already saw happening in surface waters of shelf stations closer to the Greenlandic coast. Similar to other regions of the Arctic (Kanna et al., 2014; Nakanowatari et al., 2007), the progressive melting and retreat of sea ice alters biogeochemical cycles of carbon and trace elements as well as the biological productivity in Baffin Bay and Davis Strait.

4.5 Influence of freshwater runoff from coastal sources on biogeochemical properties

The influence of coastal freshwater runoff on the chemical composition of surface waters was demonstraded by statistical analysis (refer to Sect. 4.1.2) and is evident in minimum salinity values (refer to Sect. 3.1) in surface waters of stations 6, 11, and 17. Stations 6 and 11 are located close to the mouth of the Kangerlussuaq Fjord and the Nassuttooq Fjord, which receive glacial and riverine freshwater draining from the GIS (Monteban et al., 2020). Station 17 is located in Disko Bay, approximately 70 km from the mouth of the Ilulissat Icefjord/Jakobshavn Isbræ system, where glacially modified waters form a buoyant coastal current outside the fjord (Beaird et al., 2017). Minimum salinity values in surface waters coincide with higher macronutrient concentrations (refer to Sect. 3.2). A modeling study by Møller *et al.* (2023) has shown that part of the macronutrient input into Disko Bay is directly coupled to freshwater runoff as a source. Other mechanisms that replenish marine-sourced nutrients from deeper water into the photic zone are vertical mixing fueled by wind and tide (Møller et al.,

https://doi.org/10.5194/egusphere-2025-291
Preprint. Discussion started: 11 February 2025

2023) or via the estuarine upwelling circulation forced by the glacier's freshwater input (Williams et al., 2021). Our results suggest that the continued replenishment of macronutrients into the photic zone of Disko Bay can sustain PP into the summer season, which is evident by high oxygen and low AOU concentrations in surface waters of station 17 (refer to Sect. 3.1). This has large implications on the carbonate system and the uptake of CO_2, which is reflected by low Revelle factors and low pCO_2 values in surface waters of Disko Bay (refer to Sect. 3.4). A similar observation for the Godthåbsfjord system in south Greenland revealed biological processes to be the most important drivers of CO_2 uptake, resulting in low pCO_2 concentrations in surface waters of the shelf area (Meire et al., 2015). Our results highlight that nutrient cycling in Disko Bay is strongly driven by GIS-derived freshwater input, which stimulates PP and creates an important sink for CO_2 long into the summer season.

Apart from the Disko Bay area, the surface water of stations closest to the coast of Greenland were corrosive with lower buffering capacities (refer to Sect. 3.4). Glacial freshwater from the GIS is known to have a strong AT dilution effect relative to CT, which impacts the buffering capacity of surface waters, resulting in lower Ω Aragonite saturation states and pH values (Henson et al., 2023; Burgers et al., 2024). The acidification of surface waters can be mitigated by PP, which removes CT from the photic zone and thus increases pH and Ω Aragonite (Chierici and Fransson, 2009), as seen for the Disko Bay area. Surface waters of coastal stations showed negative AOU values, indicating CT drawdown by PP. Simultaneously, extremely low NOx values (< LOQ) were present, suggesting that PP was reaching a limit due to nutrient depletion. This could explain lower pH values coupled with higher Revelle factors and pCO_2 values, as the AT dilution effect caused by the GIS freshwater input is no longer compensated for by CT removal through biological processes. Our results indicate that surface waters along west Greenland become more susceptible to acidification through the input of poorly buffered glacial freshwater as the summer season progresses and PP decreases. Our results agree well with Henson *et al.* (2023), who observed AT dilution from glacial meltwater to drive corrosive conditions in surface waters of the Greenlandic coast, causing an overall decrease in Ω Aragonite and pH (refer to Sect. 3.4).

Besides the cycling of macronutrients and carbon, the distribution of trace elements is influenced by coastal freshwater input. Overall, the surface water concentrations of dMn, dFe, dCo, dNi, and dCu were highest close to the coast and decreased with distance along each transect. For stations 11 and 12 (mouth of Nassuttooq Fjord) as well as station 17 (Disko Bay, Ilulissat Icefjord) this trend was especially pronounced, reflecting the freshwater runoff from the GIS with a distinct chemical composition (refer to Sect. 4.2.3). Our work is confirmed by previous findings from different regions around Greenland, that suggest the freshwater flux from the GIS to be a source of dMn, dFe, dCo, dNi, and dCu (Chen et al., 2022; Krause et al., 2021; Hawkings et al., 2020; Krisch et al., 2022a; Colombo et al., 2020). Surface water concentrations of dNi in Disko Bay remained relatively constant, whereas stations at the mouth of Nassuttooq Fjord exhibited higher concentrations. A similar observation was done by Krause *et al.* (2021), who related varying dNi along coastal transects to outcrops of Ni-rich minerals across West Greenland. The input of bioactive trace elements, e.g., dMn, dFe, and dCo, via GIS freshwater runoff has been suggested to stimulate primary productivity in the surrounding shelf areas (Bhatia et al., 2013; Hawkings et al., 2020). Our

https://doi.org/10.5194/egusphere-2025-291
Preprint. Discussion started: 11 February 2025

study provides further evidence that freshwater from the GIS could support biological processes by supplying bioactive trace elements.

5 Summary and Conclusion

The distribution of macronutrients, carbonate system species, and dissolved trace elements on the west Greenland shelf is highly dynamic and influenced by the complex interplay between physicochemical drivers, major ocean currents, sea ice melting, and terrestrial freshwater runoff from the GIS. The internal cycling of chemical constituents in the water column is driven by conservative mixing, with freshwater either being a source (dCu) or causing dilution (AT, CT, and dV) of parameter concentrations. Furthermore, we observed biological processes determining the pelagic flux of macronutrients, trace elements (dFe, dNi, and dCd) and carbonate system parameters. The long residence time of deep and bottom waters in Baffin Bay, along with an enclosed bathymetry that restricts circulation, facilitated the accumulation of remineralized nutrients and CT, which drove corrosive conditions and Ω Aragonite undersaturation in deep waters of southern Baffin Bay. Thus, the benthic ecosystem of the west Greenland shelf is potentially vulnerable to future ocean acidification and suppression of $CaCO_3$ saturation states. The distribution of trace elements in the study area was diverse and depended on both the intrinsic chemical behavior of each element and extrinsic factors such as biological processes (uptake and remineralization) or local sources (e.g., coastal runoff, sea ice, benthic processes). We described conservative (dV, dCu), nutrient-type (dFe, dNi, and dCd) and scavenged-type (dMn, dFe, dCo, dNi, and dCu) profiles, which correspond well with previously published data in the Arctic. Additionally, an increase in dMn, dFe, dCo, and dNi concentrations was noticeable for deep water shelf stations, which we relate to benthic fluxes at the sediment-water interface. We hypothesize that this return flux decreased with increasing distance from the Greenlandic coast as the amount of exported biogenic and terrigenous material available for remineralization and reversible scavenging also decreased. Further studies looking into Baffin Bay sediments are needed to disclose benthic fluxes of trace elements and reactions occurring therein. Our study provides a first insight into the importance of benthic inputs for trace element cycling on the west Greenland shelf and Baffin Bay.

The distribution of chemical constituents in the water column across the west Greenland shelf is mainly influenced by the opposing directions of the BIC and the WGC and their respective water masses. The southward-moving AW combines winter-cooled water in Baffin Bay with inflow of cold and fresh Arctic Ocean water of Pacific-origin through the CAA. We characterized this water mass as cold and fresh, exhibiting high nutrient contents and high CT:AT ratios due to lower biological activity and the inflow of additional CT transported through the CAA to Baffin Bay. Elevated concentrations of dFe, dMn, dCo, dNi, and dCu were present in AW because of the CAA outflow into Baffin Bay. In contrast, the northward-moving WGSW integrates freshwater of Arctic-origin from East Greenland that mixes with meltwater from the GIS. This water mass dominated the upper water column on the shelf, which we characterized as warm and fresh, highly productive, and therefore exhibiting low nutrient concentrations. Below the WGSW lies the warm and salty WGIW, which originates in the North Atlantic. This water mass is dominated by the remineralization of OM, leading to the enrichment of nutrients and carbon. We

https://doi.org/10.5194/egusphere-2025-291
Preprint. Discussion started: 11 February 2025

described the gradual mixing of all three water masses along the shelf by using the latitudinal distribution of dPb, influenced by elevated dPb waters from the North Atlantic and low dPb waters from the CAA.

Our study provides evidence that the progressive melting and retreat of sea ice alters the biological productivity as well as biogeochemical cycles of carbon and trace elements in surface waters of southern Baffin Bay. The east-to-west direction of sea ice retreat during spring and summer caused a significant gradient in nutrient concentrations. Nutrients were low in highly productive shelf waters along the eastern side of the west Greenland coast, while nutrients were higher towards the west of southern Baffin Bay because of the prolonged sea ice cover. The timing of this study enabled us to capture the beginning of a phytoplankton bloom in areas that were previously covered by sea ice but where nutrients had not yet been consumed. Additionally, sea ice meltwater provided additional AT to surface waters, likely through the dissolution of ikaite. This geochemical buffer was offset by the presence of excess CT, potentially from organic carbon remineralization under the ice and the additional CT input through the CAA to Baffin Bay. Overall, sea ice meltwater and the inflow of Pacific-origin waters lowered AT relative to CT and are responsible for higher pCO_2 and lower pH and Ω Aragonite values in surface waters. Once the sea ice melt facilitated bloom fully develops and CT is removed by PP, higher pH and Ω Aragonite values could be expected along the sea ice edge. Furthermore, we observed sea ice meltwater as a source of dFe, dCo, dNi, dCu, and dCd to southern Baffin Bay surface waters. As an additional source of bioactive trace elements, this could maintain and prolong ice-edge blooms.

We observed freshwater runoff from the GIS influencing the chemical composition of coastal waters along west Greenland, especially in Disko Bay and at the mouth of the Nassuttooq Fjord. In the Disko Bay area, GIS-derived freshwater input replenished macronutrients in the photic zone, stimulating PP and creating an important sink for CO_2 long into the summer season. The supply of bioactive trace elements via GIS freshwater runoff, could further support biological processes in the surrounding shelf areas. However, in areas along the coastline where PP was reaching a limit due to low nutrient concentrations, surface waters became more susceptible to acidification through the input of poorly buffered glacial freshwater. This work successfully captured a high-resolution, large-scale snapshot of various water column parameters across the west Greenland shelf during July. However, we were not able to resolve any seasonal variations, which can only be provided by time series studies. We believe that higher temporal monitoring is necessary to fully assess the consequences of climate change in this climate-sensitive region.

https://doi.org/10.5194/egusphere-2025-291
Preprint. Discussion started: 11 February 2025

Data availability statement

The data set for the carbonate system and dissolved trace elements can be found online at: https://doi.org/10.5281/zenodo.14235091 (Schmidt et al., 2024).

Supplement link

The supplements to this article can be found online at: XXX

Author contribution

Claudia E. Schmidt: Conceptualization, Formal Analysis, Investigation, Methodology, Data curation, Visualization, Writing – original draft
Tristan Zimmermann: Writing – review & editing
Katarzyna Koziorowska-Makuch: Investigation, Writing – review & editing
Daniel Proefrock: Resources, Supervision, Writing – review & editing
Helmuth Thomas: Funding acquisition, Project administration, Resources, Writing – review & editing

Declaration of competing interest

The authors declare that they have no conflict of interest.

Acknowledgement

The authors would like to thank the captain and crew of RV Dana for their support during the sampling campaign in 2021. Special thanks to Camilla Svensen and Ulrike Dietrich (both University of Tromsø) for the collection of the nutrient samples and Colin Stedmon and his team (Technical University of Denmark) for the nutrient analysis.

Financial support

This project has received funding from the European Union's Horizon 2020 research and innovation program under Grant Agreement No. 869383 (ECOTIP) and the European Union's Horizon 2023 research and innovation program under Grant Agreement No. 101136480 (SEA-Quester). The project was made possible through the program "Changing Earth – Sustaining our Future" (Subtopic 4.1) within the Helmholtz Association.

https://doi.org/10.5194/egusphere-2025-291
Preprint. Discussion started: 11 February 2025

References

Aguilar-Islas, A. M., Rember, R. D., Mordy, C. W., and Wu, J.: Sea ice-derived dissolved iron and its potential influence on the spring algal bloom in the Bering Sea, Geophysical Research Letters, 35, doi:10.1029/2008GL035736, 2008.

Akima, H., and Gebhardt, A.: akima: Interpolation of Irregularly and Regularly Spaced Data, CRAN [code], https://CRAN.R-project.org/package=akima, 2022.

Aksenov, Y., Karcher, M., Proshutinsky, A., Gerdes, R., de Cuevas, B., Golubeva, E., Kauker, F., Nguyen, A. T., Platov, G. A., Wadley, M., Watanabe, E., Coward, A. C., and Nurser, A. J.: Arctic pathways of Pacific Water: Arctic Ocean Model Intercomparison experiments, Journal of geophysical research. Oceans, 121, 27-59, doi:10.1002/2015jc011299, 2016.

Arnone, V., Santana-Casiano, J. M., González-Dávila, M., Planquette, H., Sarthou, G., Gerringa, L. J. A., and González, A. G.: Natural copper-binding ligands in the Arctic Ocean. The influence of the Transpolar Drift (GEOTRACES GN04), Frontiers in Marine Science, 10, doi:10.3389/fmars.2023.1306278, 2023.

Azetsu-Scott, K., Clarke, A., Falkner, K., Hamilton, J., Jones, E. P., Lee, C., Petrie, B., Prinsenberg, S., Starr, M., and Yeats, P.: Calcium carbonate saturation states in the waters of the Canadian Arctic Archipelago and the Labrador Sea, Journal of Geophysical Research: Oceans, 115, doi:10.1029/2009JC005917, 2010.

Bates, N. R., and Mathis, J. T.: The Arctic Ocean marine carbon cycle: evaluation of air-sea CO_2 exchanges, ocean acidification impacts and potential feedbacks, Biogeosciences, 6, 2433-2459, doi:10.5194/bg-6-2433-2009, 2009.

Bates, N. R., Mathis, J. T., and Cooper, L. W.: Ocean acidification and biologically induced seasonality of carbonate mineral saturation states in the western Arctic Ocean, Journal of Geophysical Research: Oceans, 114, doi:10.1029/2008JC004862, 2009.

Beaird, N., Straneo, F., and Jenkins, W.: Characteristics of meltwater export from Jakobshavn Isbræ and Ilulissat Icefjord, Annals of Glaciology, 58, 107-117, doi:10.1017/aog.2017.19, 2017.

Beaupré-Laperrière, A., Mucci, A., and Thomas, H.: The recent state and variability of the carbonate system of the Canadian Arctic Archipelago and adjacent basins in the context of ocean acidification, Biogeosciences, 17, 3923-3942, doi:10.5194/bg-17-3923-2020, 2020.

Bhatia, M. P., Kujawinski, E. B., Das, S. B., Breier, C. F., Henderson, P. B., and Charette, M. A.: Greenland meltwater as a significant and potentially bioavailable source of iron to the ocean, Nature Geoscience, 6, 274-278, doi:10.1038/ngeo1746, 2013.

Bi, H., Zhang, Z., Wang, Y., Xu, X., Liang, Y., Huang, J., Liu, Y., and Fu, M.: Baffin Bay sea ice inflow and outflow: 1978–1979 to 2016–2017, The Cryosphere, 13, 1025-1042, doi:10.5194/tc-13-1025-2019, 2019.

Bruyant, F., Amiraux, R., Amyot, M.-P., Archambault, P., Artigue, L., Barbedo de Freitas, L., Bécu, G., Bélanger, S., Bourgain, P., Bricaud, A., Brouard, E., Brunet, C., Burgers, T., Caleb, D., Chalut, K., Claustre, H., Cornet-Barthaux, V., Coupel, P., Cusa, M., Cusset, F., Dadaglio, L., Davelaar, M., Deslongchamps, G., Dimier, C., Dinasquet, J., Dumont, D., Else, B., Eulaers, I., Ferland, J., Filteau, G., Forget, M.-H., Fort, J., Fortier, L., Galí-Tapías, M., Gallinari, M., Garbus, S.-E., Garcia,

https://doi.org/10.5194/egusphere-2025-291
Preprint. Discussion started: 11 February 2025

N., Gérikas Ribeiro, C., Gombault, C., Gourvil, P., Goyens, C., Grant, C., Grondin, P.-L., Guillot, P., Hillion, S., Hussherr, R., Joux, F., Joy-Warren, H., Joyal, G., Kieber, D., Lafond, A., Lagunas, J., Lajeunesse, P., Lalande, C., Larivière, J., Le Gall, F., Leblanc, K., Leblanc, M., Legras, J., Levesque, K., Lewis, K.-M., Leymarie, E., Leynaert, A., Linkowski, T., Lizotte, M., Lopes dos Santos, A., Marec, C., Marie, D., Massé, G., Massicotte, P., Matsuoka, A., Miller, L., Mirshak, S., Morata, N., Moriceau, B., Morin, P.-I., Morisset, S., Mosbech, A., Mucci, A., Nadaï, G., Nozais, C., Obernosterer, I., Paire, T., Panagiotopoulos, C., Parenteau, M., Pelletier, N., Picheral, M., Quéguiner, B., Raimbault, P., Ras, J., Rehm, E., Ribot Lacosta, L., Rontani, J.-F., Saint-Béat, B., Sansoulet, J., Sardet, N., Schmechtig, C., Sciandra, A., Sempéré, R., Sévigny, C., Toullec, J., Tragin, M., Tremblay, J.-E., Trottier, A.-P., Vaulot, D., Vladoiu, A., Xue, L., Yunda-Guarin, G., and Babin, M.: The Green Edge cruise: following the evolution of the Arctic phytoplankton spring bloom, from ice-covered to open waters, SEANOE [data set], doi:10.17882/86417, 2022.

Bundy, R. M., Tagliabue, A., Hawco, N. J., Morton, P. L., Twining, B. S., Hatta, M., Noble, A. E., Cape, M. R., John, S. G., Cullen, J. T., and Saito, M. A.: Elevated sources of cobalt in the Arctic Ocean, Biogeosciences, 17, 4745-4767, doi:10.5194/bg-17-4745-2020, 2020.

Burgers, T. M., Azetsu-Scott, K., Myers, P. G., Else, B. G. T., Miller, L. A., Rysgaard, S., Chan, W., Tremblay, J.-É., and Papakyriakou, T.: Unraveling the Biogeochemical Drivers of Aragonite Saturation State in Baffin Bay: Insights From the West Greenland Continental Shelf, Journal of Geophysical Research: Oceans, 129, e2024JC021122, doi:10.1029/2024JC021122, 2024.

Chen, X.-G., Krisch, S., Al-Hashem, A., Hopwood, M. J., Rutgers van der Loeff, M. M., Huhn, O., Lodeiro, P., Steffens, T., and Achterberg, E. P.: Dissolved, Labile, and Total Particulate Trace Metal Dynamics on the Northeast Greenland Shelf, Global Biogeochemical Cycles, 36, e2022GB007528, doi:10.1029/2022GB007528, 2022.

Chierici, M., and Fransson, A.: Calcium carbonate saturation in the surface water of the Arctic Ocean: undersaturation in freshwater influenced shelves, Biogeosciences, 6, 2421-2431, doi:10.5194/bg-6-2421-2009, 2009.

Colombo, M., Rogalla, B., Myers, P. G., Allen, S. E., and Orians, K. J.: Tracing Dissolved Lead Sources in the Canadian Arctic: Insights from the Canadian GEOTRACES Program, ACS Earth and Space Chemistry, 3, 1302-1314, doi:10.1021/acsearthspacechem.9b00083, 2019.

Colombo, M., Jackson, S. L., Cullen, J. T., and Orians, K. J.: Dissolved iron and manganese in the Canadian Arctic Ocean: On the biogeochemical processes controlling their distributions, Geochimica et Cosmochimica Acta, 277, 150-174, doi:10.1016/j.gca.2020.03.012, 2020.

Colombo, M., Rogalla, B., Li, J., Allen, S. E., Orians, K. J., and Maldonado, M. T.: Canadian Arctic Archipelago Shelf-Ocean Interactions: A Major Iron Source to Pacific Derived Waters Transiting to the Atlantic, Global Biogeochemical Cycles, 35, e2021GB007058, doi:10.1029/2021GB007058, 2021.

Curry, B., Lee, C. M., and Petrie, B.: Volume, Freshwater, and Heat Fluxes through Davis Strait, 2004–05, Journal of Physical Oceanography, 41, 429-436, doi:10.1175/2010JPO4536.1, 2011.

https://doi.org/10.5194/egusphere-2025-291
Preprint. Discussion started: 11 February 2025

Curry, B., Lee, C. M., Petrie, B., Moritz, R. E., and Kwok, R.: Multiyear Volume, Liquid Freshwater, and Sea Ice Transports through Davis Strait, 2004–10, Journal of Physical Oceanography, 44, 1244-1266, doi:10.1175/JPO-D-13-0177.1, 2014.

Dickson, A. G., and Millero, F. J.: A comparison of the equilibrium constants for the dissociation of carbonic acid in seawater media, Deep Sea Research Part A. Oceanographic Research Papers, 34, 1733-1743, doi:10.1016/0198-0149(87)90021-5, 1987.

Dickson, A. G.: Standard potential of the reaction: AgCl(s) + 12H2(g) = Ag(s) + HCl(aq), and and the standard acidity constant of the ion HSO4− in synthetic sea water from 273.15 to 318.15 K, The Journal of Chemical Thermodynamics, 22, 113-127, doi:10.1016/0021-9614(90)90074-Z, 1990.

DIN e.V.: DIN 32645: Chemical analysis–Decision limit, detection limit and determination limit under repeatability conditions–Terms, methods, evaluation, doi:10.31030/1465413, 2008.

Ebeling, A., Zimmermann, T., Klein, O., Irrgeher, J., and Pröfrock, D.: Analysis of Seventeen Certified Water Reference Materials for Trace and Technology-Critical Elements, Geostandards and Geoanalytical Research, 46, 351-378, doi:10.1111/ggr.12422, 2022.

Evans, L. K., and Nishioka, J.: Accumulation processes of trace metals into Arctic sea ice: distribution of Fe, Mn and Cd associated with ice structure, Marine Chemistry, 209, 36-47, doi:10.1016/j.marchem.2018.11.011, 2019.

Finley, A., Banerjee, S., and Hjelle, Ø.: MBA: Multilevel B-Spline Approximation, CRAN [code], https://CRAN.R-project.org/package=MBA, 2022.

Foukal, N. P., and Pickart, R. S.: Moored Observations of the West Greenland Coastal Current along the Southwest Greenland Shelf, Journal of Physical Oceanography, 53, 2619-2632, doi:10.1175/JPO-D-23-0104.1, 2023.

Fransson, A., Chierici, M., Miller, L. A., Carnat, G., Shadwick, E., Thomas, H., Pineault, S., and Papakyriakou, T. N.: Impact of sea-ice processes on the carbonate system and ocean acidification at the ice-water interface of the Amundsen Gulf, Arctic Ocean, Journal of Geophysical Research: Oceans, 118, 7001-7023, doi:10.1002/2013JC009164, 2013.

Fransson, A., Chierici, M., Nomura, D., Granskog, M. A., Kristiansen, S., Martma, T., and Nehrke, G.: Effect of glacial drainage water on the CO2 system and ocean acidification state in an Arctic tidewater-glacier fjord during two contrasting years, Journal of Geophysical Research: Oceans, 120, 2413-2429, doi:10.1002/2014JC010320, 2015.

GEBCO Bathymetric Compilation Group 2023: The GEBCO_2023 Grid - a continuous terrain model of the global oceans and land, NERC EDS British Oceanographic Data Centre NOC [data set], doi:10.5285/f98b053b-0cbc-6c23-e053-6c86abc0af7b, 2023.

GEOTRACES Intermediate Data Product Group: The GEOTRACES Intermediate Data Product 2021 version 2 (IDP2021v2), NERC EDS British Oceanographic Data Centre NOC [data set], doi:10.5285/ff46f034-f47c-05f9-e053-6c86abc0dc7e, 2023.

Gerringa, L. J. A., Rijkenberg, M. J. A., Slagter, H. A., Laan, P., Paffrath, R., Bauch, D., Rutgers van der Loeff, M., and Middag, R.: Dissolved Cd, Co, Cu, Fe, Mn, Ni, and Zn in the Arctic Ocean, Journal of Geophysical Research: Oceans, 126, e2021JC017323, doi:10.1029/2021JC017323, 2021.

https://doi.org/10.5194/egusphere-2025-291
Preprint. Discussion started: 11 February 2025

Haine, T. W. N., Curry, B., Gerdes, R., Hansen, E., Karcher, M., Lee, C., Rudels, B., Spreen, G., de Steur, L., Stewart, K. D., and Woodgate, R.: Arctic freshwater export: Status, mechanisms, and prospects, Global and Planetary Change, 125, 13-35, doi:10.1016/j.gloplacha.2014.11.013, 2015.

Hansen, H. P., and Koroleff, F.: Determination of nutrients, in: Methods of Seawater Analysis, 159-228, doi:10.1002/9783527613984.ch10, 1999.

Hawkings, J., Wadham, J., Tranter, M., Telling, J., Bagshaw, E., Beaton, A., Simmons, S.-L., Chandler, D., Tedstone, A., and Nienow, P.: The Greenland Ice Sheet as a hot spot of phosphorus weathering and export in the Arctic, Global Biogeochemical Cycles, 30, 191-210, doi:10.1002/2015GB005237, 2016.

Hawkings, J. R., Wadham, J. L., Tranter, M., Lawson, E., Sole, A., Cowton, T., Tedstone, A. J., Bartholomew, I., Nienow, P., Chandler, D., and Telling, J.: The effect of warming climate on nutrient and solute export from the Greenland Ice Sheet, Geochemical Perspectives Letters, 1, 94-104, doi:10.7185/geochemlet.1510, 2015.

Hawkings, J. R., Wadham, J., Benning, L., Hendry, K., Tranter, M., Tedstone, A., Nienow, P., and Raiswell, R.: Ice sheets as a missing source of silica to the polar oceans, Nature Communications, 8, 14198, doi:10.1038/ncomms14198, 2017.

Hawkings, J. R., Skidmore, M. L., Wadham, J. L., Priscu, J. C., Morton, P. L., Hatton, J. E., Gardner, C. B., Kohler, T. J., Stibal, M., Bagshaw, E. A., Steigmeyer, A., Barker, J., Dore, J. E., Lyons, W. B., Tranter, M., and Spencer, R. G. M.: Enhanced trace element mobilization by Earth's ice sheets, Proceedings of the National Academy of Sciences, 117, 31648-31659, doi:10.1073/pnas.2014378117, 2020.

Hendry, K. R., Huvenne, V. A. I., Robinson, L. F., Annett, A., Badger, M., Jacobel, A. W., Ng, H. C., Opher, J., Pickering, R. A., Taylor, M. L., Bates, S. L., Cooper, A., Cushman, G. G., Goodwin, C., Hoy, S., Rowland, G., Samperiz, A., Williams, J. A., Achterberg, E. P., Arrowsmith, C., Alexander Brearley, J., Henley, S. F., Krause, J. W., Leng, M. J., Li, T., McManus, J. F., Meredith, M. P., Perkins, R., and Woodward, E. M. S.: The biogeochemical impact of glacial meltwater from Southwest Greenland, Progress in Oceanography, 176, 102126, doi:10.1016/j.pocean.2019.102126, 2019.

Henson, H. C., Holding, J. M., Meire, L., Rysgaard, S., Stedmon, C. A., Stuart-Lee, A., Bendtsen, J., and Sejr, M.: Coastal freshening drives acidification state in Greenland fjords, Science of The Total Environment, 855, 158962, doi:10.1016/j.scitotenv.2022.158962, 2023.

Hölemann, J. A., Schirmacher, M., and Prange, A.: Dissolved and Particulate Major and Trace Elements in Newly Formed Ice from the Laptev Sea (Transdrift III, October 1995), in: Land-Ocean Systems in the Siberian Arctic: Dynamics and History, edited by: Kassens, H., Bauch, H. A., Dmitrenko, I. A., Eicken, H., Hubberten, H.-W., Melles, M., Thiede, J., and Timokhov, L. A., Springer Berlin Heidelberg, Berlin, Heidelberg, 101-111, doi:10.1007/978-3-642-60134-7_11, 1999.

Hopwood, M. J., Carroll, D., Dunse, T., Hodson, A., Holding, J. M., Iriarte, J. L., Ribeiro, S., Achterberg, E. P., Cantoni, C., Carlson, D. F., Chierici, M., Clarke, J. S., Cozzi, S., Fransson, A., Juul-Pedersen, T., Winding, M. H. S., and Meire, L.: Review article: How does glacier discharge affect marine biogeochemistry and primary production in the Arctic?, The Cryosphere, 14, 1347-1383, doi:10.5194/tc-14-1347-2020, 2020.

https://doi.org/10.5194/egusphere-2025-291
Preprint. Discussion started: 11 February 2025

Jensen, L. T., Cullen, J. T., Jackson, S. L., Gerringa, L. J. A., Bauch, D., Middag, R., Sherrell, R. M., and Fitzsimmons, J. N.: A Refinement of the Processes Controlling Dissolved Copper and Nickel Biogeochemistry: Insights From the Pan-Arctic, Journal of Geophysical Research: Oceans, 127, e2021JC018087, doi:10.1029/2021JC018087, 2022.

Jones, E. M., Chierici, M., Menze, S., Fransson, A., Ingvaldsen, R. B., and Lødemel, H. H.: Ocean acidification state variability of the Atlantic Arctic Ocean around northern Svalbard, Progress in Oceanography, 199, 102708, doi:10.1016/j.pocean.2021.102708, 2021.

Jones, E. P., Coote, A. R., and Levy, E. M.: Effect of sea ice meltwater on the alkalinity of seawater, ISSN: 0022-2402, 1983.

Juranek, L.: Changing Biogeochemistry of the Arctic Ocean: Surface Nutrient and CO2 Cycling in a Warming, Melting North, Oceanography, doi:10.5670/oceanog.2022.120, 2022.

Juul-Pedersen, T., Arendt, K. E., Mortensen, J., Blicher, M. E., Søgaard, D. H., and Rysgaard, S.: Seasonal and interannual phytoplankton production in a sub-Arctic tidewater outlet glacier fjord, SW Greenland, Marine Ecology Progress Series, 524, 27-38, https://www.int-res.com/abstracts/meps/v524/p27-38/, 2015.

Kanna, N., Toyota, T., and Nishioka, J.: Iron and macro-nutrient concentrations in sea ice and their impact on the nutritional status of surface waters in the southern Okhotsk Sea, Progress in Oceanography, 126, 44-57, doi:10.1016/j.pocean.2014.04.012, 2014.

Krause, J., Hopwood, M. J., Höfer, J., Krisch, S., Achterberg, E. P., Alarcón, E., Carroll, D., González, H. E., Juul-Pedersen, T., Liu, T., Lodeiro, P., Meire, L., and Rosing, M. T.: Trace Element (Fe, Co, Ni and Cu) Dynamics Across the Salinity Gradient in Arctic and Antarctic Glacier Fjords, Frontiers in Earth Science, 9, doi:10.3389/feart.2021.725279, 2021.

Krawczyk, D. W., Kryk, A., Juggins, S., Burmeister, A., Pearce, C., Seidenkrantz, M. S., Moros, M., Høyer, J. L., Kuijpers, A., and Witkowski, A.: Spatio-temporal changes in ocean conditions and primary production in Baffin Bay and the Labrador Sea, Palaeogeography, Palaeoclimatology, Palaeoecology, 563, 110175, doi:10.1016/j.palaeo.2020.110175, 2021.

Krisch, S., Hopwood, M. J., Roig, S., Gerringa, L. J. A., Middag, R., Rutgers van der Loeff, M. M., Petrova, M. V., Lodeiro, P., Colombo, M., Cullen, J. T., Jackson, S. L., Heimbürger-Boavida, L.-E., and Achterberg, E. P.: Arctic – Atlantic Exchange of the Dissolved Micronutrients Iron, Manganese, Cobalt, Nickel, Copper and Zinc With a Focus on Fram Strait, Global Biogeochemical Cycles, 36, e2021GB007191, doi:10.1029/2021GB007191, 2022a.

Krisch, S., Huhn, O., Al-Hashem, A., Hopwood, M. J., Lodeiro, P., and Achterberg, E. P.: Quantifying Ice-Sheet Derived Lead (Pb) Fluxes to the Ocean; A Case Study at Nioghalvfjerdsbræ, Geophysical Research Letters, 49, e2022GL100296, doi:10.1029/2022GL100296, 2022b.

Lafond, A., Leblanc, K., Queguiner, B., Moriceau, B., Leynaert, A., Cornet, V., Legras, J., Ras, J., Parenteau, M., Garcia, N., Babin, M., and Tremblay, J.-E.: Late spring bloom development of pelagic diatoms in Baffin Bay, Elementa-science Of The Anthropocene, 7, doi:10.1525/elementa.382, 2019.

Lehmann, N., Kienast, M., Granger, J., Bourbonnais, A., Altabet, M. A., and Tremblay, J.-É.: Remote Western Arctic Nutrients Fuel Remineralization in Deep Baffin Bay, Global Biogeochemical Cycles, 33, 649-667, doi:10.1029/2018GB006134, 2019.

https://doi.org/10.5194/egusphere-2025-291
Preprint. Discussion started: 11 February 2025

Li, Y.-H., and Tsui, T.-F.: The solubility of CO2 in water and sea water, Journal of Geophysical Research (1896-1977), 76, 4203-4207, doi:10.1029/JC076i018p04203, 1971.

Marsay, C. M., Aguilar-Islas, A., Fitzsimmons, J. N., Hatta, M., Jensen, L. T., John, S. G., Kadko, D., Landing, W. M., Lanning, N. T., Morton, P. L., Pasqualini, A., Rauschenberg, S., Sherrell, R. M., Shiller, A. M., Twining, B. S., Whitmore, L. M., Zhang, R., and Buck, C. S.: Dissolved and particulate trace elements in late summer Arctic melt ponds, Marine Chemistry, 204, 70-85, doi:10.1016/j.marchem.2018.06.002, 2018.

McConnell, J. R., and Edwards, R.: Coal burning leaves toxic heavy metal legacy in the Arctic, Proceedings of the National Academy of Sciences, 105, 12140-12144, doi:10.1073/pnas.0803564105, 2008.

Measures, C. I.: The role of entrained sediments in sea ice in the distribution of aluminium and iron in the surface waters of the Arctic Ocean, Marine Chemistry, 68, 59-70, doi:10.1016/S0304-4203(99)00065-1, 1999.

Mehrbach, C., Culberson, C. H., Hawley, J. E., and Pytkowicx, R. M.: MEASUREMENT OF THE APPARENT DISSOCIATION CONSTANTS OF CARBONIC ACID IN SEAWATER AT ATMOSPHERIC PRESSURE1, Limnology and Oceanography, 18, 897-907, doi:10.4319/lo.1973.18.6.0897, 1973.

Meire, L., Søgaard, D. H., Mortensen, J., Meysman, F. J. R., Soetaert, K., Arendt, K. E., Juul-Pedersen, T., Blicher, M. E., and Rysgaard, S.: Glacial meltwater and primary production are drivers of strong CO_2 uptake in fjord and coastal waters adjacent to the Greenland Ice Sheet, Biogeosciences, 12, 2347-2363, doi:10.5194/bg-12-2347-2015, 2015.

Meire, L., Mortensen, J., Meire, P., Juul-Pedersen, T., Sejr, M. K., Rysgaard, S., Nygaard, R., Huybrechts, P., and Meysman, F. J. R.: Marine-terminating glaciers sustain high productivity in Greenland fjords, Glob Chang Biol, 23, 5344-5357, doi:10.1111/gcb.13801, 2017.

Miller, L., Davelaar, M., Caleb, D., Mucci, A., Burgers, T., Ahmed, M., and Irish, V.: Dissolved inorganic carbon (DIC), total alkalinity, stable oxygen isotope (O-18), temperature, salinity, dissolved oxygen and other parameters measured from discrete samples and profile observations during the Canadian Coast Guard Ship Amundsen ArcticNet cruise (EXPOCODE 18DL20160603, Leg 1 and Leg 2) in the Eastern Canadian Arctic, Baffin Bay, Nares Strait, Lancaster Sound, Barrow Strait and Coronation Gulf from 2016-06-03 to 2016-08-23 (NCEI Accession 0217304), NOAA National Centers for Environmental Information [data set], doi:10.25921/719e-qr37, 2020.

Møller, E. F., Christensen, A., Larsen, J., Mankoff, K. D., Ribergaard, M. H., Sejr, M., Wallhead, P., and Maar, M.: The sensitivity of primary productivity in Disko Bay, a coastal Arctic ecosystem, to changes in freshwater discharge and sea ice cover, Ocean Sci., 19, 403-420, doi:10.5194/os-19-403-2023, 2023.

Monteban, D., Pedersen, J. O. P., and Nielsen, M. H.: Physical oceanographic conditions and a sensitivity study on meltwater runoff in a West Greenland fjord: Kangerlussuaq, Oceanologia, 62, 460-477, doi:10.1016/j.oceano.2020.06.001, 2020.

Mouginot, J., Rignot, E., Bjørk, A. A., van den Broeke, M., Millan, R., Morlighem, M., Noël, B., Scheuchl, B., and Wood, M.: Forty-six years of Greenland Ice Sheet mass balance from 1972 to 2018, Proceedings of the National Academy of Sciences, 116, 9239-9244, doi:10.1073/pnas.1904242116, 2019.

https://doi.org/10.5194/egusphere-2025-291
Preprint. Discussion started: 11 February 2025

Nakanowatari, T., Ohshima, K. I., and Wakatsuchi, M.: Warming and oxygen decrease of intermediate water in the northwestern North Pacific, originating from the Sea of Okhotsk, 1955–2004, Geophysical Research Letters, 34, doi:10.1029/2006GL028243, 2007.

Niebauer, H. J., Alexander, V., and Henrichs, S. M.: A time-series study of the spring bloom at the Bering Sea ice edge I. Physical processes, chlorophyll and nutrient chemistry, Continental Shelf Research, 15, 1859-1877, doi:10.1016/0278-4343(94)00097-7, 1995.

Oksman, M., Kvorning, A. B., Larsen, S. H., Kjeldsen, K. K., Mankoff, K. D., Colgan, W., Andersen, T. J., Nørgaard-Pedersen, N., Seidenkrantz, M. S., Mikkelsen, N., and Ribeiro, S.: Impact of freshwater runoff from the southwest Greenland Ice Sheet on fjord productivity since the late 19th century, The Cryosphere, 16, 2471-2491, doi:10.5194/tc-16-2471-2022, 2022.

Perrette, M., Yool, A., Quartly, G. D., and Popova, E. E.: Near-ubiquity of ice-edge blooms in the Arctic, Biogeosciences, 8, 515-524, doi:10.5194/bg-8-515-2011, 2011.

Pierrot, D., Wallace, D., and Lewis, E.: MS Excel program developed for CO2 system calculations, Carbon Dioxide Information Analysis Center [code], doi:10.3334/CDIAC/otg.CO2SYS_XLS_CDIAC105a, 2011.

Posit team: RStudio: Integrated Development Environment for R, Posit Software, PBC [code], http://www.posit.co/, 2023.

Przibilla, A., Iwainski, S., Zimmermann, T., and Pröfrock, D.: Impact of storage temperature and filtration method on dissolved trace metal concentrations in coastal water samples, Water Environment Research, 95, e10922, doi:10.1002/wer.10922, 2023.

R Core Team: R: A Language and Environment for Statistical Computing, R Foundation for Statistical Computing [code], https://www.R-project.org/, 2022.

Revelle, W.: psych: Procedures for Psychological, Psychometric, and Personality Research, CRAN [code], https://CRAN.R-project.org/package=psych, 2024.

Ruacho, A., Richon, C., Whitby, H., and Bundy, R. M.: Sources, sinks, and cycling of dissolved organic copper binding ligands in the ocean, Communications Earth & Environment, 3, 263, doi:10.1038/s43247-022-00597-1, 2022.

Rysgaard, S., Bendtsen, J., Delille, B., Dieckmann, G. S., Glud, R. N., Kennedy, H., Mortensen, J., Papadimitriou, S., Thomas, D. N., and Tison, J.-L.: Sea ice contribution to the air–sea CO_2 exchange in the Arctic and Southern Oceans, Tellus B: Chemical and Physical Meteorology, doi:10.1111/j.1600-0889.2011.00571.x, 2011.

Rysgaard, S., Glud, R. N., Lennert, K., Cooper, M., Halden, N., Leakey, R. J. G., Hawthorne, F. C., and Barber, D.: Ikaite crystals in melting sea ice – implications for CO_2 and pH levels in Arctic surface waters, The Cryosphere, 6, 901-908, doi:10.5194/tc-6-901-2012, 2012.

Sarmiento, J. L., and Gruber, N.: Ocean Biogeochemical Dynamics, Princeton University Press, ISBN: 9780691017075, 2006.

Schmidt, C. E., Pröfrock, D., and Thomas, H.: ECOTIP Dana Cruise July 2021 - Alkalinity (AT), dissolved inorganic carbon (CT) and dissolved trace elements, Zenodo [data set], doi:10.5281/zenodo.14235091, 2024.

Schnetger, B., and Lehners, C.: Determination of nitrate plus nitrite in small volume marine water samples using vanadium(III)chloride as a reduction agent, Marine Chemistry, 160, 91-98, doi:10.1016/j.marchem.2014.01.010, 2014.

https://doi.org/10.5194/egusphere-2025-291
Preprint. Discussion started: 11 February 2025

Seo, H., Kim, G., Kim, T., Kim, I., Ra, K., and Jeong, H.: Trace elements (Fe, Mn, Co, Cu, Cd, and Ni) in the East Sea (Japan Sea): Distributions, boundary inputs, and scavenging processes, Marine Chemistry, 239, 104070, doi:10.1016/j.marchem.2021.104070, 2022.

Shadwick, E. H., Thomas, H., Chierici, M., Else, B., Fransson, A., Michel, C., Miller, L. A., Mucci, A., Niemi, A., Papakyriakou, T. N., and Tremblay, J.-É.: Seasonal variability of the inorganic carbon system in the Amundsen Gulf region of the southeastern Beaufort Sea, Limnology and Oceanography, 56, 303-322, doi:10.4319/lo.2011.56.1.0303, 2011a.

Shadwick, E. H., Thomas, H., Gratton, Y., Leong, D., Moore, S. A., Papakyriakou, T., and Prowe, A. E. F.: Export of Pacific carbon through the Arctic Archipelago to the North Atlantic, Continental Shelf Research, 31, 806-816, doi:10.1016/j.csr.2011.01.014, 2011b.

Shadwick, E. H., Trull, T. W., Thomas, H., and Gibson, J. A. E.: Vulnerability of Polar Oceans to Anthropogenic Acidification: Comparison of Arctic and Antarctic Seasonal Cycles, Scientific Reports, 3, 2339, doi:10.1038/srep02339, 2013.

Sherwood, O. A., Davin, S. H., Lehmann, N., Buchwald, C., Edinger, E. N., Lehmann, M. F., and Kienast, M.: Stable isotope ratios in seawater nitrate reflect the influence of Pacific water along the northwest Atlantic margin, Biogeosciences, 18, 4491-4510, doi:10.5194/bg-18-4491-2021, 2021.

Smrzka, D., Zwicker, J., Bach, W., Feng, D., Himmler, T., Chen, D., and Peckmann, J.: The behavior of trace elements in seawater, sedimentary pore water, and their incorporation into carbonate minerals: a review, Facies, 65, 41, doi:10.1007/s10347-019-0581-4, 2019.

Spreen, G., Kaleschke, L., and Heygster, G.: Sea ice remote sensing using AMSR-E 89-GHz channels, Journal of Geophysical Research: Oceans, 113, doi:10.1029/2005JC003384, 2008.

Strass, V. H., and Nöthig, E. M.: Seasonal shifts in ice edge phytoplankton blooms in the Barents Sea related to the water column stability, Polar Biology, 16, 409-422, doi:10.1007/BF02390423, 1996.

Tang, C. C. L., Ross, C. K., Yao, T., Petrie, B., DeTracey, B. M., and Dunlap, E.: The circulation, water masses and sea-ice of Baffin Bay, Progress in Oceanography, 63, 183-228, doi:10.1016/j.pocean.2004.09.005, 2004.

Tovar-Sánchez, A., Duarte, C. M., Alonso, J. C., Lacorte, S., Tauler, R., and Galbán-Malagón, C.: Impacts of metals and nutrients released from melting multiyear Arctic sea ice, Journal of Geophysical Research: Oceans, 115, doi:10.1029/2009JC005685, 2010.

Tremblay, J.-É., Gratton, Y., Carmack, E. C., Payne, C. D., and Price, N. M.: Impact of the large-scale Arctic circulation and the North Water Polynya on nutrient inventories in Baffin Bay, Journal of Geophysical Research: Oceans, 107, 26-21-26-14, doi:10.1029/2000JC000595, 2002.

Tynan, E., Clarke, J. S., Humphreys, M. P., Ribas-Ribas, M., Esposito, M., Rérolle, V. M. C., Schlosser, C., Thorpe, S. E., Tyrrell, T., and Achterberg, E. P.: Physical and biogeochemical controls on the variability in surface pH and calcium carbonate saturation states in the Atlantic sectors of the Arctic and Southern Oceans, Deep Sea Research Part II: Topical Studies in Oceanography, 127, 7-27, doi:10.1016/j.dsr2.2016.01.001, 2016.

https://doi.org/10.5194/egusphere-2025-291
Preprint. Discussion started: 11 February 2025

Vernet, M., Ellingsen, I., Marchese, C., Bélanger, S., Cape, M., Slagstad, D., and Matrai, P. A.: Spatial variability in rates of net primary production (NPP) and onset of the spring bloom in Greenland shelf waters, Progress in Oceanography, 198, 102655, doi:10.1016/j.pocean.2021.102655, 2021.

Vieira, L. H., Achterberg, E. P., Scholten, J., Beck, A. J., Liebetrau, V., Mills, M. M., and Arrigo, K. R.: Benthic fluxes of trace metals in the Chukchi Sea and their transport into the Arctic Ocean, Marine Chemistry, 208, 43-55, doi:10.1016/j.marchem.2018.11.001, 2019.

Whitmore, L. M., Morton, P. L., Twining, B. S., and Shiller, A. M.: Vanadium cycling in the Western Arctic Ocean is influenced by shelf-basin connectivity, Marine Chemistry, 216, 103701, doi:10.1016/j.marchem.2019.103701, 2019.

Williams, P. L., Burgess, D. O., Waterman, S., Roberts, M., Bertrand, E. M., and Bhatia, M. P.: Nutrient and Carbon Export From a Tidewater Glacier to the Coastal Ocean in the Canadian Arctic Archipelago, Journal of Geophysical Research: Biogeosciences, 126, e2021JG006289, doi:10.1029/2021JG006289, 2021.

Wouters, B., and Sasgen, I.: Increasing freshwater fluxes from the Greenland Ice Sheet observed from space, Oceanography, 35, 103-105, doi:10.5670/oceanog.2022.125, 2022.

Wu, Y., Hain, M. P., Humphreys, M. P., Hartman, S., and Tyrrell, T.: What drives the latitudinal gradient in open-ocean surface dissolved inorganic carbon concentration?, Biogeosciences, 16, 2661-2681, doi:10.5194/bg-16-2661-2019, 2019.